Construction and Building Materials 259 (2020) 120395

Contents lists available at ScienceDirect

Construction and Building Materials

journal homepage: www.elsevier.com/locate/conbuildmat

Experimental and analytical investigation of high performance concrete beams reinforced with hybrid bars and polyvinyl alcohol fibers

Mohamed Said *, T.S. Mustafa, Ali S. Shanour *, Mostafa M. Khalil

Faculty of Engineering (Shoubra), Benha University, Egypt

HIGHLIGHTS

- Discussion of the performance of concrete beams containing ECC.
- PVA fibers enhanced the cracking load, ultimate capacity.
- Hybrid bars exhibited an improvement in the stiffness of the concrete beams.
- The inclusion of hybrid bars delayed the appearance of the first crack.
- PVA exhibits an improvement in the ductility factor and strain ductility.
- Nominal flexural strength and flexural rigidity were assessed.

ARTICLE INFO

Article history:
Received 28 January 2020
Received in revised form 14 June 2020
Accepted 24 July 2020

Keywords:
Hybrid bars
Schemes
ECC
PVA fibers
Flexural rigidity
strain Ductility

ABSTRACT

This paper investigates the flexural performance of engineered cementitious composite (ECC) concrete beams reinforced with innovative hybrid bars. Hybrid bars combine the advantages of both FRP and steel bars in enhancing the ultimate strength, ductility, and corrosion resistance compared with pure FRP or steel bars. Twelve half-scale ECC-concrete beams were tested to study the flexure behaviour under four-points loading test using polyvinyl alcohol (PVA) ECC fibers. Polyvinyl alcohol (PVA) fibers were used in the ECC mix for this purpose. The experimental variables are the hybrid reinforcement ratios (0.85%, 1.26%, and 1.7%), PVA fiber ratio (0.0%, 0.75%, and 1.5%) and hybrid schemes (hybrid and GFRP bars). The test results showed significant enhancement in the capacity of ECC concrete beams reinforced with hybrid bars or hybrid schemes. The achieved enhancements are 12% and 27% for PVA ratio of 0.75% and 1.5% respectively. In the presence of PVA fibers, the ultimate strain of the bars is higher than that registered in the absence of PVA fibers. Non-linear finite element analysis (NLFEA) was carried out to validate the experimental results. The NLFEA is adequately simulating the experimental results. Nominal flexural strength and flexural rigidity were assessed with the experimental test results and validated with 77 available ECC-concrete beams from the literature. The validation proved that the assessments of the nominal flexural strength and flexural rigidity are performed well in the prediction. Finally, a comprehensive sensitivity study is conducted to illustrate the effect of PVA-ECC on the flexural rigidity of the beams. The experimental evidence presented in the current study demonstrates the feasibility and plausible future of the novel hybrid bars and PVA fibers especially for marine and waterfront concrete structures.

1. Introduction

Recently, concrete technology has been undergoing rapid development, resulting in the production of a new concept of high-performance concrete (HPC). High-performance concrete has been primarily used in tunnels, bridges and tall buildings. Investigating the behaviour of HPC for the structural members was reported [1–4]. The advantages gained by using HPC include reduction of the size of concrete members, high early strength, durability, and higher elastic modulus. In addition, service life is more than 100 years, high toughness and tensile strength [4]. Over the years, the innovation of fiber reinforcing materials has been investigated. The contribution of short steel fibers in the improvement of the structural performance of concrete structures was studied [5–7]. This improvement has continued using the extension of varied

* Corresponding authors.
E-mail addresses: mohamed.abdelghaffar@feng.bu.edu.eg (M. Said), tarek.mohamed@feng.bu.edu (T.S. Mustafa), ali.shnor@feng.bu.edu.eg (A.S. Shanour), Mostafa.khalil@feng.bu.edu.eg (M.M. Khalil).

https://doi.org/10.1016/j.conbuildmat.2020.120395
0950-0618/

Nomenclature

A_c	area of the compression zone.
A_{et}	area of ECC concrete in the tension side.
A_f	the reinforcing area of FRP bars in tension
A_{hr}	area of the hybrid reinforcement bars
A_s	the reinforcing area of steel reinforcement bars in tension
A_t	total cross-section area of the beam
a	depth of the rectangular stress block
b	width of the cross-section
C	depth of compression zone in concrete
Cc	the compression force of concrete
D	flexural rigidity of the beam
$D_{,ECC}$	flexural rigidity of ECC-concrete beams
$D_{,RC}$	flexural rigidity of reinforced concrete beams
DF	ductility factor
$DF_{exp.}$	experimental ductility factor
$DF_{NL.}$	predicted ductility factor from NLFEA
DF_R	ductility factor of the control beam
d	depth of the beam
d'	distance from the center of the tension bars to the concrete tension edge
E	Modulus of elasticity
E_c	Modulus of elasticity for concrete
E_f	Modulus of elasticity for GFRP bars
E_{hr}	Modulus of elasticity for hybrid bars
E_s	Modulus of elasticity for steel bars
e	depth of ECC concrete in the tension side
F_{be}	bond efficiency of the fiber
f_{cr}	rupture modulus of concrete
f_c'	cylindrical compressive strength of the concrete
f_{ecp}'	cylindrical compressive strength of ECC concrete
f_f	tensile strength of FRP bars
f_{hr}	tensile strength of the hybrid bar
f_u	ultimate strength of the reinforcing bars
f_y	yield strength of the reinforcing bars
I	energy absorption
I_{cr}	the cracked moment of inertia
I_{eff}	the effective moment of inertia
$I_{eff,\ exp.}$	the experimental effective moment of inertia
$I_{eff,\ n.}$	the nominal effective moment of inertia
$I_{exp.}$	experimental energy absorption
I_g	the gross moment of inertia
$I_{NL.}$	predicted energy absorption from NLFEA
I_R	energy absorption of the control beam
K	initial stiffness
$K_{\text{-exp.}}$	experimental initial stiffness
$K_{\text{-}NL.}$	predicted initial stiffness from NLFEA
K_R	initial stiffness of the control beam
k_1	constant value = 3×10^8
k_2	constant value = 10^7
k_3	constant value = 1.46×10^5
L	length of the beam
l_f	length of PVA fibers
M_a	applied moment at the yield load level
M_{cr}	flexural cracking moment
$M_{\ exp.}$	experimental moment strength
$M_{n.}$	nominal flexural strength
m	the modular ratio of PVA-ECC fiber
n_f	the modular ratio of GFRP bars
n_{hr}	the modular ratio of hybrid bars
n_s	the modular ratio of steel bars
P_{cr}	cracking load
$P_{cr\text{-exp.}}$	experimental cracking load
$P_{cr\text{-}NL.}$	predicted cracking load from NLFEA
$P_{cr\text{-}R}$	the cracking load of the control beam
P_u	ultimate load-carrying capacity
$P_{u\text{-exp.}}$	experimental load-carrying capacity
$P_{u\text{-}NL.}$	predicted load-carrying capacity from NLFEA
$P_{u\text{-}R}$	the ultimate load-carrying capacity of the control beam
P_y	load at the yield level
$P_{y\text{-exp.}}$	experimental load at the yield level
$P_{y\text{-}NL.}$	predicted load at the yield level from NLFEA
$P_{y\text{-}R}$	load at the yield level of the control beam
T_{et}	tension force of ECC concrete
T_s	tension force of steel reinforcement bars
T_f	tension force of FRP bars
T_{hr}	tension force of hybrid bars
t	depth of the cross-section
V_f	Volume of PVA fibers
X	flexural shear span
y_t	depth of the neutral axis measured from the tension side
Z	the depth of the compression zone measured from the neutral axis
α	coefficient depends on the design code
β	factor relating depth of equivalent rectangular compressive stress block to neutral axis depth
β_d	parameter accounted for the bond properties and elastic modulus of FRP bars
$\boldsymbol{\varepsilon_{hr}}$	the tensile strain of the hybrid bar
$\boldsymbol{\varepsilon_{hr}}$, exp.	the experimental tensile strain of the reinforcing bars
$\boldsymbol{\varepsilon_{hr}}_{NL.}$	predicted tensile strain of the reinforcing bars from NLFEA
$\boldsymbol{\varepsilon_{hr}}$, $n.$	the nominal tensile strain of the reinforcing bars from NLFEA
$\boldsymbol{\varepsilon_y}$	the tensile strain of the reinforcing bars at the yield level
μ_s	strain ductility
$\mu_{s,\ NL.}$	predicted strain ductility from NLFEA
ρ	density of the material
ρ_f	reinforcement ratio of GFRP bars = $(A_f/b.d)$
ρ_{hr}	reinforcement ratio of hybrid bars = $(A_{hr}/b.d)$
$\rho_{hr\text{-}Sch}$	reinforcement ratio of hybrid schemes
ρ_{PVA}	percent by volume of PVA fibers
ρ_s	reinforcement ratio of steel reinforcement bars = $(A_s/b.d)$
ρ_t	total reinforcement ratio = $(\rho_s + \rho_f + \rho_{hr})$
δ_u	deflection at the ultimate level
$\delta_{u\text{-exp.}}$	experimental deflection at the ultimate level
$\delta_{u\text{-}NL.}$	predicted deflection at the ultimate level from NLFEA
$\delta_{u\text{-}R}$	deflection at the ultimate level of the control beam
δ_y	deflection at the yield level
$\delta_{y\text{-exp.}}$	experimental deflection at the yield level
$\delta_{y\text{-}NL.}$	predicted deflection at the yield level from NLFEA
$\delta_{y\text{-}R}$	deflection at the yield level of the control beam
σ_c	effective compressive strength of concrete
σ_{ec}	effective compressive strength of ECC concrete
σ_{et}	effective tensile strength of ECC concrete
ϕ_f	diameter of PVA fibers

fiber types such as glass, carbon, and synthetics [8–10]. Polyvinyl alcohol (PVA) fibers considered a type of promising synthetics fibers that were innovated by Herrmann, et al. [11] and were devolved in Japan by Dr. Sakurada's [12]. Compared with the different types of fibers, PVA fiber has many advantages including resistance to corrosion, high strain capacity and ductility. Also, PVA fiber provides strong bonding with the cement matrix and cracking control over the long term. Accordingly, using PVA fibers in

develop HPC would reduce the brittle behaviour of the traditional concrete and enhance the flexure performance of the concrete structures.

The effect of PVA fibers inclusion on the mechanical properties of ECC concrete was studied [13–17]. Hamoush et al. [13] investigated the stress–strain behaviour in tension and compression for specimens with PVA. The test results showed that PVA fibers delayed the development of micro-cracks and the composite demonstrated greater strength and crack resistance than normal concrete. Also, the failure mechanism of the specimens subjected to axial compression exhibited no strain-softening response and the descending branch after peak stress was almost vertical. Moreover, Adding PVA fibers to normal concrete matrix enhanced the post-cracking response which led to improved ductility and toughness. Mechanical properties for specimens with PVA and PP fibers have been studied in compression and tension by Xiang et al. [16]. The test results displayed that the compressive strength and the elastic modulus of specimens with PP fibers were lower than specimens with PVA fibers. In addition, specimens with PVA fibers showed higher tensile strength and ultimate strain when compared to specimens with PP fibers. Investigations on the behaviour of concrete structures containing ECC were studied [18–22]. Experimental test results for twelve RC beams containing ECC were conducted by Shanour, et al. [18]. The main parameters were the steel reinforcement ratio (ρ_s), the height of ECC implementation in the cross-section of the beams, type of fibers (polyvinyl alcohol (PVA) and polypropylene (PP)) and volume of fiber (V_f). The deflection behaviour, cracking and the capacities of the tested beams were evaluated. Specimens with PVA fibers showed better behaviour than specimens with PP fibers. ECC was heavily used in non-structural applications mainly for thin slabs sections. There are gaps in the research regarding their performance in other structural elements.

The rapid corrosion of steel reinforcement bars is considered one of the main causes for reducing the service life of RC structures. To achieve the requirements of ultimate limit state and durability for these structures, steel reinforcement bars should be replaced or coated with non-corrosive materials. Fiber-reinforced polymer (FRP) bars were used as an alternative material to resolve the corrosion problem of steel reinforcement bars. The common types of fibers are carbon, glass, and aramid. FRP bars provide high specific strength and also good resistance to corrosion. Investigations on the behaviour of concrete beams reinforced with FRP bars were studied [23–28]. FRP bars have linear stress–strain behaviour under tension and up to failure with a lower elastic modulus and no ductility compared to steel reinforcement bars [29]. This behaviour causes large deflections, crack widths and brittle failure. Moreover, the observed investigated failure modes from the experimental test results were compression failures. Based on these reasons, FRP reinforcement is not recommended for moment resistance frames [30–33].

To enhance the ductility, flexural capacity and providing more corrosion protection for RC structures. Several researchers proposed the concept of combining steel bars with FRP bars (hybrid schemes) in RC structures [34–40]. In the hybrid schemes, FRP bars are located at the corners of the concrete elements and steel reinforcement bars are placed inside the element for more protection. Using steel reinforcing bars improves the ductility permitting the tension failure and prevents the occurrence of compression failure for RC structures. At the same time, the FRP bars increase the capacity of the RC structures [41–45]. An experimental investigation on the hybrid reinforced beams containing ECC was presented by Jie, et al. [34]. The ratio of the height of ECC in the cross section to the total height of the cross section of the specimens and combinations of FRP and steel reinforcements were the main investigated parameters. Test results showed that cracking, yield, ultimate moments, and the stiffness of hybrid and ECC beams were improved compared with reinforced concrete beams with the same reinforcement.

An innovative reinforcing material for the flexural structural element is created which called hybrid reinforcement bars. A less common area of research relates to investigating the potential of using two different materials (FRP or steel) together as reinforcement in a hybrid bar [46–49]. These systems seek to capitalize on the higher axial stiffness of one material like conventional steel, while still benefitting from the corrosion resistance of FRP. Forty-eight specimens of the hybrid reinforcement bars were experimentally tested under uniaxial tensile test by Minkwan et al., [46] to predict the tensile strength and the elastic modulus of the hybrid bar. The test results showed a higher modulus of elasticity than the GFRP bar. The mentioned previous research works were limited to investigate the behaviour of the hybrid bars only. For that reason, the investigation of the performance of concrete members reinforced with hybrid bars is required.

This paper aims to introduce a more effective system by using PVA-ECC concrete beams reinforced with innovative hybrid bars to overcome the corrosion problems and the brittle behaviour of the traditional concrete beams. The fundamental mechanical properties of the hybrid bars were evaluated and verified with the other works. Twelve half-scale PVA-ECC concrete beams reinforced with hybrid bars and hybrid schemes were experimentally tested under four-point loads. The main parameters were the hybrid reinforcement ratios, PVA fiber volume (V_f), and hybrid schemes (hybrid and GFRP) bars. The cracking load, maximum load and load–deflection curves were discussed and the load–strain curves of the hybrid bars were presented. Moreover, the cracks pattern and failure modes have been observed. NLFEA was performed to simulate the tested beams using ANSYS software [50]. Finally, nominal flexural strength and flexural rigidity of PVA-ECC concrete beams reinforced with hybrid bars were validated with the experimental results.

2. Experimental program

2.1. Hybrid bars manufacturing and testing

The hybrid and GFRP bars were produced by the authors using a steel bar (steel core), glass fiber roving, and resin. Up to 70 glass fibers roving to manufacture GFRP bars with 12 mm nominal diameter were used while, 22 glass fibers roving were used to manufacture the outer GFRP surface of the hybrid bar with a 14 mm nominal diameter. Fig. 1 shows the produced hybrid bar and GFRP bar.

The mechanical properties of the six hybrid bars, GFRP bars and steel bars were investigated by a machine of 1000 kN capacity. The tensile stress–strain curves for six hybrid bars are presented in Fig. 2. Comparison between the tensile stress–strain curves for steel bar, GFRP bar and the average tensile stress–strain curve for six hybrid bars are shown in Fig. 3. The average tensile stress–strain curves showed a bi-linear behaviour and acceptable ductility against the brittle failure of GFRP bars. Moreover, higher elastic modulus and lower tensile strength were recorded for hybrid bars when compared to GFRP bars. The slope of the stress–strain curves is determined as the average tensile modulus of elasticity of the bars.

The idealized stress–strain curve for the six hybrid bars has been assumed to simulate the bilinear best fitting of the experimental tensile stress–strain curves for the hybrid bars. The idealized tensile stress of the hybrid bar can be calculated by the following formula:

$$f_{hr} = k_1 \varepsilon_{hr}{}^3 - k_2 \varepsilon_{hr}{}^2 + k_3 \varepsilon_{hr} \quad (1)$$

(a) 14 mm Hybrid Bars

(b) Ribbed 12 mm GFRP Bars

Fig. 1. Produced GFRP and Hybrid Bars.

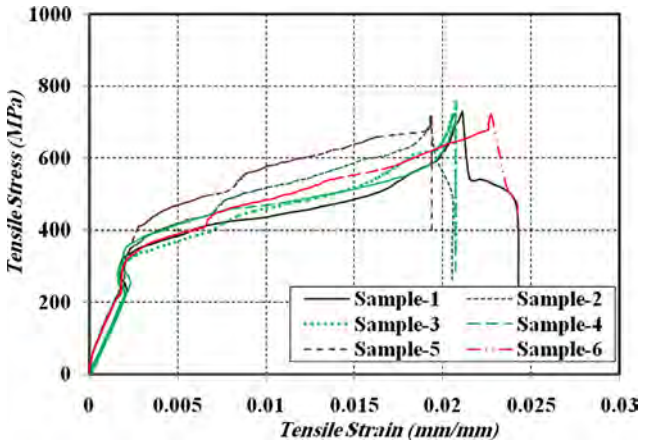

Fig. 2. Tensile Stress-Strain Curves for the Hybrid Bars.

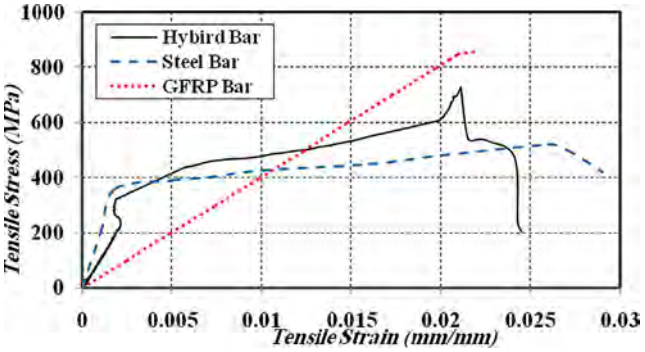

Fig. 3. Comparison between Tensile Stress-Strain Curves for Steel Bar, GFRP Bar and Average Stress-Strain Curve for Hybrid Bar.

The values of the constants k_1, k_2, and k_3 have been obtained from the regression analysis using Datafit software [51], these values are (3×10^8), (10^7), and (1.46×10^5) respectively. The idealized tensile stress–strain curves for the hybrid bars were verified with the tensile test results from the literature [46,48] as shown in Fig. 4. The comparison showed good agreements between the produced hybrid bars in this research and the produced hybrid bars in [46,48].

2.2. Materials and specimens

Twelve half-scale concrete beams reinforced with hybrid bars and containing ECC were designed as a simply supported span with an adequate amount of longitudinal and shear reinforcement. The study investigated the influence of the fundamental parameters on the flexural behaviour of concrete beams. The investigated parameters include the hybrid reinforcement ratios, the volumetric ratio of PVA (V_f), and hybrid schemes (hybrid and GFRP bars). Four beams labeled as (B1, B4, B7, and B10) were poured without PVA fibers as control beams for comparison. Another group of four beams were totally casted with a PVA volume ratio of 0.75%. The last group of four beams were poured with a PVA volume ratio of 1.5%. The properties of PVA as provided by the supplier are listed in Table 1. The shape of the PVA fibers is shown in Fig. 5. Furthermore, six cylindrical specimens of dimensions 150 × 300 mm were tested to achieve the average compressive stress–strain curve for each mix. The experimental stress–strain curve for concrete specimens with and without PVA is presented in Fig. 6.

The twelve specimens were divided into four Groups (A, B, C, and D). Each group consisted of three concrete beams with different PVA volume ratios (0%, 0.75%, and 1.5%) and the same reinforcement ratio. Three different tensile reinforcement ratios (ρ_t) (0.85%, 1.26%, and 1.70%) were used. The first three Groups (A, B, and C) were reinforced with hybrid bars while Group D was reinforced with hybrid schemes of hybrid bars and GFRP bars. The average mechanical properties of the used reinforcing bars are presented in Table 2. For all tested beams, two 8 mm steel bars were used as top reinforcement to hold stirrups and 8 mm diameter stirrups @ 100 mm c/c spacing were used as shear reinforcement. The

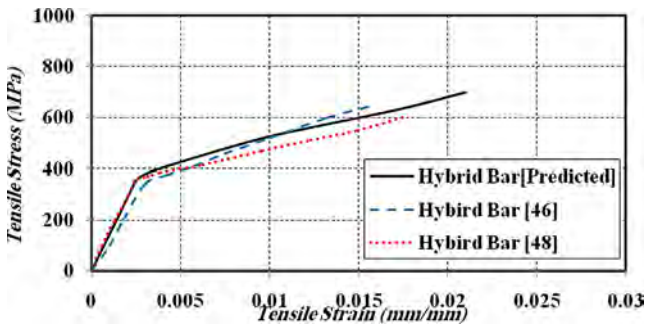

Fig. 4. Comparison of the Idealized Tensile Stress-Strain Curves for the Hybrid Bars.

Table 1
Properties of the Polyvinyl Alcohol (PVA).

Length (l_f) (mm)	Diameter (ϕ_f) (mm)	Tensile Strength (MPa)	Elastic Modulus (GPa)	Density (ρ) (g/cm^3)	Elongation (%)
12	0.04	1620	42.80	1.3	7.0

Fig. 5. Shape of Polyvinyl Alcohol Fibers (PVA).

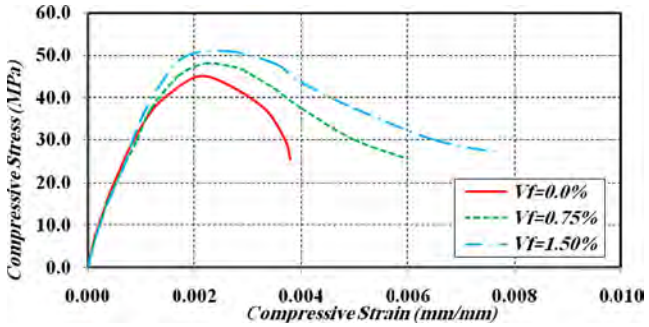

Fig. 6. Compressive Stress–strain curves for typical specimens.

geometry of the tested beams is detailed in Fig. 7 and summarized in Table 3.

The concrete strength depends primarily on the properties of the constituent materials (Portland cement, sand, coarse aggregate, water, and PVA fibers), their mix proportions and the method of their preparation, placing, compacting and curing. Table 4 presents the mix design for the concrete in the present work. (Sikament®-R4PN) high range water reducer (HRWR) and slump retaining concrete admixtures were used in the mix design.

Six cubes of dimensions 150 × 150 × 150 mm and three cylinders of dimensions 100 × 200 mm were poured from each mix and tested to evaluate the compressive strength and tensile strength of the hardened concrete respectively. Furthermore, six cylindrical specimens of dimensions 150 × 300 mm were tested to achieve the average cylindrical compressive stress–strain curve for each mix. The recorded results in Table 5 showed that the inclusion of ECC-PVA fibers slightly enhanced the compressive strength of the concrete. On the other hand, PVA fibers showed significant enhancement for tensile strength than the gained enhancement in compressive strength. Comparing with non-fibrous concrete, using 1.5% PVA improved the compressive strength and tensile strength by 7.5% and 85% respectively. Fadhil et al. [52] reported that PVA does not affect the compressive strength of the tested mixes. On the other hand, the inclusion of PVA fibers enhanced the splitting tensile strength of the specimens. Similar observations were noted by Said et al. [19] reported that using PVA fibers enhanced the tensile strength and flexural strength higher than their companions without PVA fibers.

2.3. Test setup

The beams were tested in a machine of 1000 kN capacity. The load was distributed on two plates kept with 400 mm apart. The two loads were symmetrical to the centreline of the beam. The beams were tested under load control. Strain gauges were fixed at the longitudinal reinforcement bars to measure the strain of the bars as illustrated in Figs. 8 and 9. The deflection at the centreline was recorded for every 0.5 kN increment of load using linear variable differential transformers (LVDT) fitted at the center. The cracks were mapped out during loading stages until failure.

3. Experimental results and discussion

3.1. Crack load and ultimate load

All beams were visually observed until the appearance of the first crack with recording of the corresponding first cracking load. Table 6 summarizes the observed test results. Generally, increasing

Table 2
Mechanical Properties of the Reinforcing Bars.

Reinforcement Type	Diameter (mm)	Yield Strength (f_y) N/mm^2	Ultimate Strength (f_u) N/mm^2	Young's Modulus (E) (GPa)
MS	8	240	350	200
GFRP	12	–	850	42.5
C.O.V for GFRP	–	–	5.70%	5.40%
HR	14	380	700	140
C.O.V for HR	–	4.80%	4.40%	4.20%

Note: MS = mild steel bar, GFRP = glass fiber reinforced polymer bar and HR = hybrid bar.

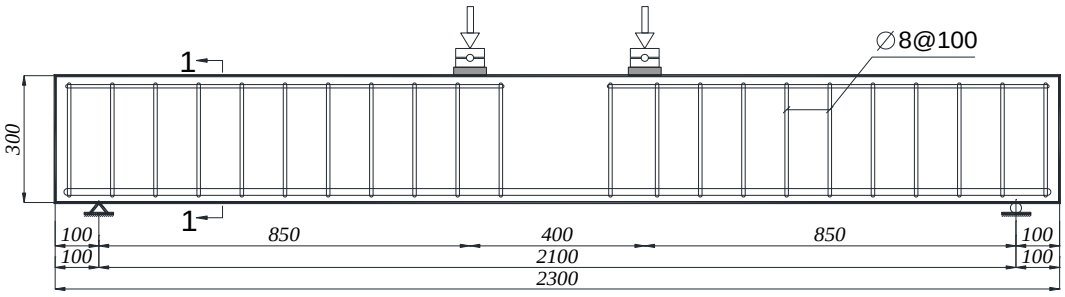

Longitudinal Section for the Tested Beams

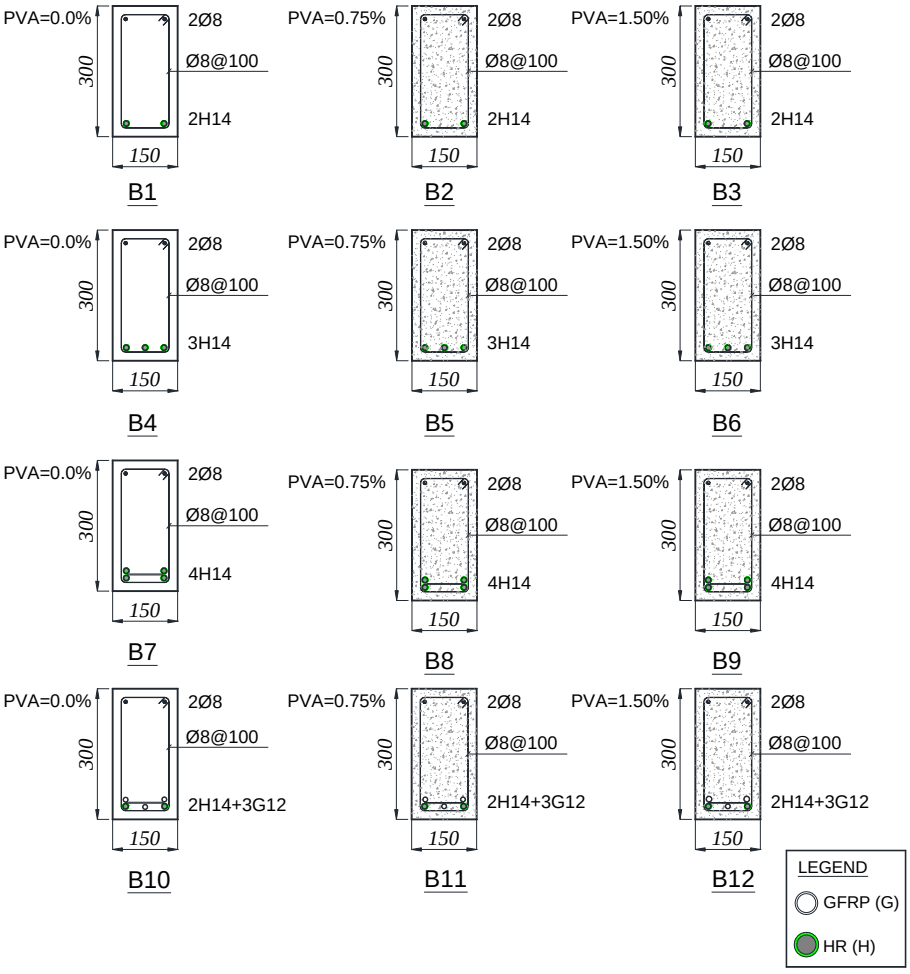

Fig. 7. Tested Beams Geometry and Details.

fiber ratio of PVA improves the behaviour of reinforced concrete beams in terms of first cracking load (P_{cr}) and ultimate load level (P_u). For beam B1 in Group (A), the inclusion of PVA fibers enhanced the crack load (P_{cr}) for B2 and B3 by 14% and 38% respectively. At the ultimate level, the load-carrying capacity improved for B2 and B3 respectively by 8% and 24%. Compared with beam B4 in Group B, the crack load (P_{cr}) was enhanced for B5 and B6 by 28% and 41% respectively. Moreover, the load-carrying capacity was enhanced by 12% and 27% for B5 and B6. For Group D, compared with the non-fibrous beam B10, the inclusion of PVA fibers with the hybrid schemes improved the crack load (P_{cr}) for B11 and B12 by 6% and 14% respectively and also enhanced the load-carrying capacity by 5% and 12% respectively. It was concluded by Jie et al. [34] that the cracking and ultimate loads of beams containing PVA fibers are higher than beams without PVA fibers.

Test results also showed an enhancement for (P_{cr}) and (P_u) by increasing the hybrid reinforcement ratio (ρ_{hr}). Reference to beam B3, increasing the hybrid reinforcement ratio enhanced (P_{cr}) for B6 and B9 respectively by 13% and 16%. Additionally, (P_u) showed an improvement by 27% and 47% for B6 and B9 respectively. Accordingly, the hybrid bars displayed the main contribution to improve the flexural capacity for the PVA-ECC concrete beams.

Table 3
Details of the Tested Beams.

Group	*Beam*	*Fiber content (PVA)V_f %*	*Bottom RFT*		*Bottom RFT Ratios*			*Stirrups (Steel bars)*	*Top RFT (Steel bars)*
			A_f GFRP	*A_{hr} HR*	*ρ_f %*	*ρ_{hr} %*	*ρ_t %*		
A	**B1**	0.00	–	2H14	–	0.85	0.85	10 ϕ 8/m'	2 ϕ 8
	B2	0.75	–	2H14	–	0.85	0.85	10 ϕ 8/m'	2 ϕ 8
	B3	1.50	–	2H14	–	0.85	0.85	10 ϕ 8/m'	2 ϕ 8
B	**B4**	0.00	–	3H14	–	1.26	1.26	10 ϕ 8/m'	2 ϕ 8
	B5	0.75	–	3H14	–	1.26	1.26	10 ϕ 8/m'	2 ϕ 8
	B6	1.50	–	3H14	–	1.26	1.26	10 ϕ 8/m'	2 ϕ 8
C	**B7**	0.00	–	4H14	–	1.70	1.70	10 ϕ 8/m'	2 ϕ 8
	B8	0.75	–	4H14	–	1.70	1.70	10 ϕ 8/m'	2 ϕ 8
	B9	1.50	–	4H14	–	1.70	1.70	10 ϕ 8/m'	2 ϕ 8
D	**B10**	0.00	3G12	2H14	0.85	0.85	1.70	10 ϕ 8/m'	2 ϕ 8
	B11	0.75	3G12	2H14	0.85	0.85	1.70	10 ϕ 8/m'	2 ϕ 8
	B12	1.50	3G12	2H14	0.85	0.85	1.70	10 ϕ 8/m'	2 ϕ 8

Table 4
Concrete Mix Proportions per One Cubic Meter.

Mix No.	**Quantity required for 1 m^3 (kg)**					**PVA-V_f (%)**
	Cement	**Sand**	**Coarse aggregate**	**Water**	**HRWR**	
1	550	620	1180	200	10	0.00
2	550	620	1180	200	15	0.75
3	550	620	1180	200	15	1.50

Table 5
Compressive and Splitting Strength.

Mix No.	**PVA-V_f (%)**	**Average Cylindrical Compressive strength (MPa)**	**C.O.V (%)**	**Average Splitting Tensile strength (MPa)**	**C.O.V (%)**
1	0.00	46.5	5.70	3.70	4.6
2	0.75	48.3	5.20	4.90	4.3
3	1.50	50.0	4.80	6.85	2.9

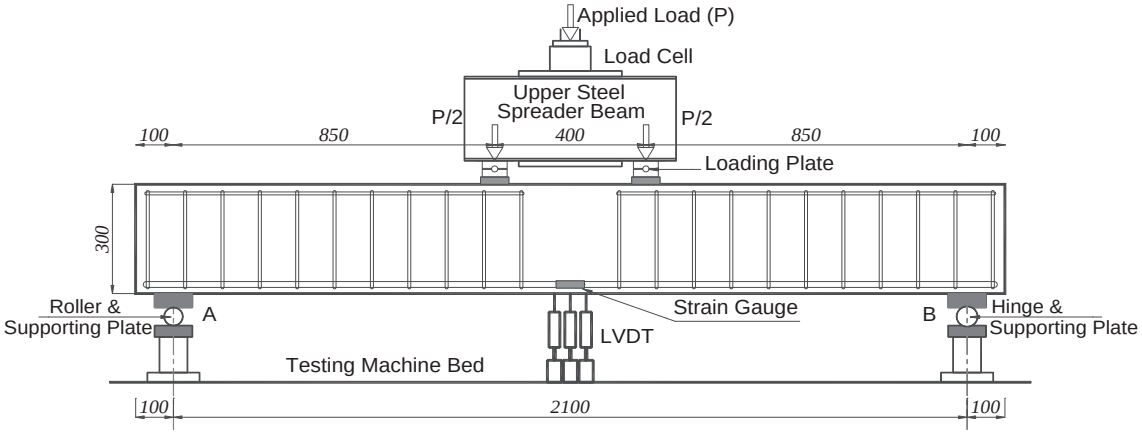

Fig. 8. Testing Setup Details.

3.2. Load-deflection curves

The experimental load–deflection curves for Groups A, B, C, and Group D are plotted in Figs. 10–13 respectively. Generally, the load–deflection curves consist of three main branches, the first branch is linear that specifies the response until the initial cracks and the second branch is also, linear fitting that represents the response until the yield of longitudinal reinforcement. After the yielding of reinforcement, increasing the deflection took place for successive loads. Beams containing PVA exhibit higher mid-span deflection before failure with extended ductile plateau more than control beams due to the strain hardening and multiple micro-cracking behaviours of PVA. To evaluate the contribution of hybrid bars and PVA fibers on the flexural performance of the tested beams, the following measurements can be observed from the load–deflection curves:

Fig. 9. Typical Beam during Testing.

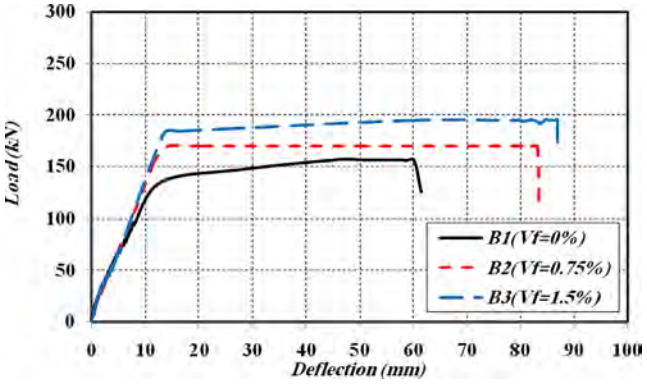

Fig. 10. Load-Deflection Curves of the Tested Beams for Group A.

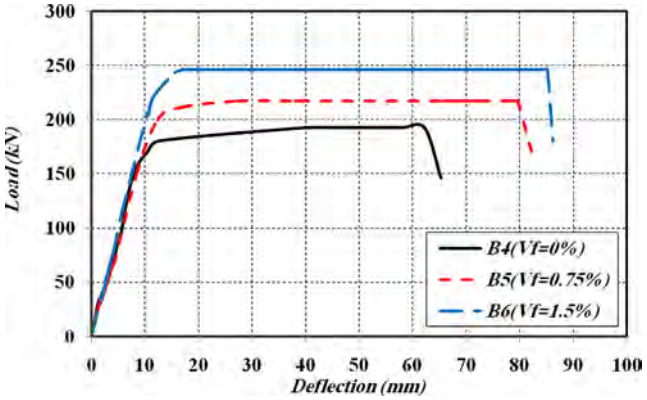

Fig. 11. Load-Deflection Curves of the Tested Beams for Group B.

3.2.1. Initial stiffness (K)

Using hybrid bars as tension reinforcement exhibit an improvement in the stiffness (K) which, can be defined as the ratio between load at yield level (P_y) to the corresponding displacement (δ_y) [19]. For the same fiber content, comparing with beam B2, increasing the hybrid reinforced ratio enhanced the stiffness for B5 and B8 by 39% and 37 respectively. On the other hand, a reduction in the stiffness was observed for beam B11 by 13%. The reduction in the stiffness occurred due to the existence of GFRP bars with lower modulus of elasticity. The provision of PVA fibers for the tested beams slightly enhanced the stiffness of beams reinforced with hybrid bars. For Group A, the observed enhancement in stiffness for B2 and B3 was 1.5% and 13% with reference to beam B1. Moreover, it was also recorded that the inclusion of PVA fiber is an effective way to enhance the stiffness of the hybrid schemes beams containing GFRP bars. Compared to beam B10, the stiffness was improved by 24% and 36% for beams B11 and B12 respectively.

3.2.2. Energy absorption (I)

Energy absorption (I) is defined as the area under the load–deflection curve. It is the function of the ultimate load (P_u) and the corresponding ultimate deflection (δ_u) [19]. It was noticed from the recorded results that, generally, the energy absorption enhanced by increasing PVA-ECC fiber content. For Group A, the energy absorption for B2 and B3 was higher than B1 by 58% and 87%. Also, for Group D, the energy absorption was improved for beams reinforced with hybrid schemes by 27% and 47% for B11 and B12 regarding beam B10. Also, energy absorption improved by increasing the hybrid bars reinforcing ratio. The energy absorption was increased for B6 and B9 by 27% and 52% compared to B3. Moreover, the inclusion of hybrid bars with GFRP bars enhanced energy absorption of B12 by 33% when compared to B3.

3.2.3. Ductility factor (DF)

Ductility factor (DF) for the tested beams can be defined as the ratio between the deflection at the ultimate level (δ_u) to the deflection at the yield level (δ_y) [18]. PVA fibers are generally showed an improvement in the ductility of the tested beams. It reaches the extreme strength in the post- cracking deformation in addition to a relatively large inelastic deformation capability. For Group A,

Table 6
Experimental Results of the Tested.

Group	Beam	Vf (%)	Experimental Test Results								Relative Experimental Results to the Control Beams							
			P_{cr} (kN)	P_y (kN)	δ_y (mm)	P_u (kN)	δ_u (mm)	K (kN/mm)	I (kN.mm)	DF	$\frac{P_{cr}}{P_{cr-R}}$	$\frac{P_y}{P_{y-R}}$	$\frac{\delta_y}{\delta_{y-R}}$	$\frac{P_u}{P_{u-R}}$	$\frac{\delta_u}{\delta_{u-R}}$	$\frac{K}{K_R}$	$\frac{I}{I_R}$	$\frac{DF}{DF_R}$
A	B1	0.00	29	135	10	157	61	13.5	8300	6.10	1.00	1.00	1.00	1.00	1.00	1.00	1.00	1.00
	B2	0.75	33	154.5	11.3	170	83	13.67	13,115	7.35	1.14	1.14	1.13	1.08	1.36	1.01	1.58	1.20
	B3	1.50	40	181	11.89	195	88	15.22	15,500	7.40	1.38	1.34	1.19	1.24	1.44	1.13	1.87	1.21
B	B4	0.00	32	155	9	193	67	17.2	11,800	7.44	1.00	1.00	1.00	1.00	1.00	1.00	1.00	1.00
	B5	0.75	41	200	10.5	217	82	19.05	16,400	7.81	1.28	1.29	1.17	1.12	1.22	1.11	1.39	1.05
	B6	1.50	45	222	11	246	86	20.18	19,600	7.82	1.41	1.43	1.22	1.27	1.28	1.17	1.66	1.05
C	B7	0.00	34	220	12	246	73	18.3	16,900	6.08	1.00	1.00	1.00	1.00	1.00	1.00	1.00	1.00
	B8	0.75	42	240	13	261	84	18.46	20,418	6.462	1.24	1.09	1.08	1.06	1.15	1.01	1.21	1.06
	B9	1.50	46	250	13.5	285	90	18.52	23,600	6.667	1.35	1.14	1.13	1.16	1.23	1.01	1.40	1.10
D	B10	0.00	35	230	23	245	66	10.0	14,100	2.87	1.00	1.00	1.00	1.00	1.00	1.00	1.00	1.00
	B11	0.75	37	248	20	258	80	12.40	17,900	4.00	1.06	1.08	0.87	1.05	1.21	1.24	1.27	1.39
	B12	1.50	40	265	19.5	273	86	13.59	20,600	4.41	1.14	1.15	0.85	1.11	1.30	1.36	1.46	1.54

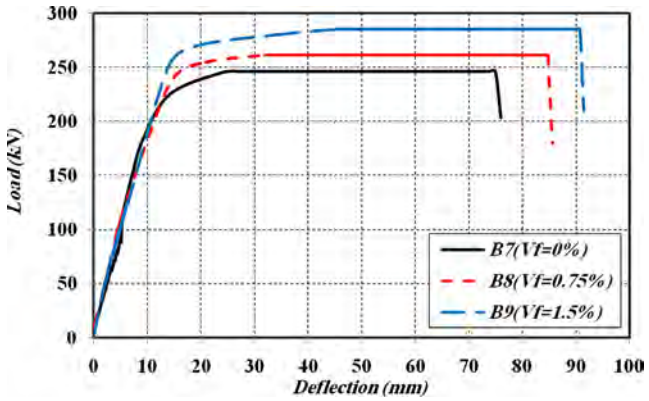

Fig. 12. Load-Deflection Curves of the Tested Beams for Group C.

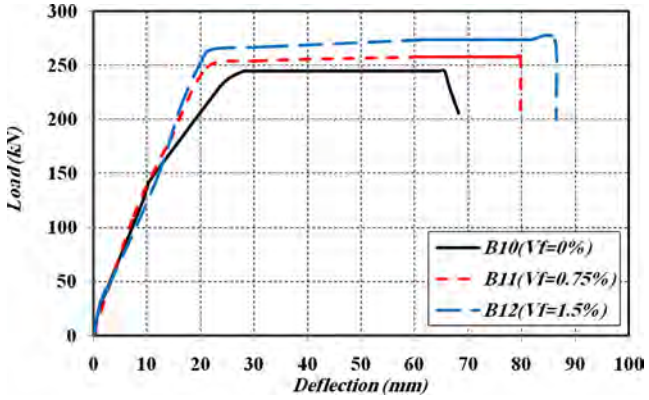

Fig. 13. Load-Deflection Curves of the Tested Beams for Group D.

compared to beam B1, the DF showed an improvement for B2 and B3 respectively by 20% and 21%. Also, significant enhancement in the DF was observed for beams B11 and B12 respectively by 39% and 54% compared to B10 in Group D. Accordingly, the inclusion of PVA fibers for beams reinforced with hybrid schemes decreases the degradation of the DF for the beams due to the brittle behaviour of GFRP bars. Meng et al. [20] observed that the ductility factor enhanced by increasing the PVA volume ratio in the PVA concrete beams.

3.3. Strains in the hybrid bars

The strains of the hybrid bars (ε_{hr}) at the ultimate level were measured and recorded in Table 7. Also, the load-hybrid strain

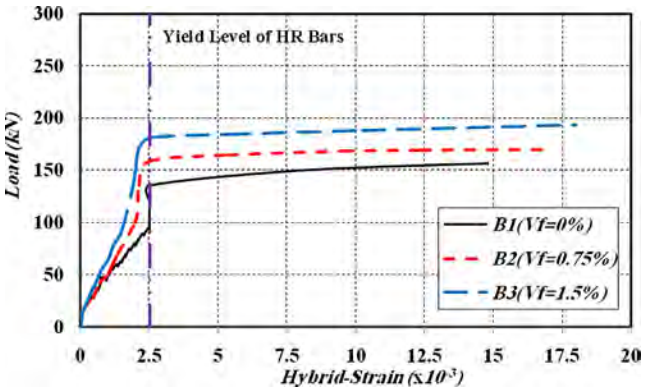

Fig. 14. Load-Hybrid Strain of the Tested Beams for Group A.

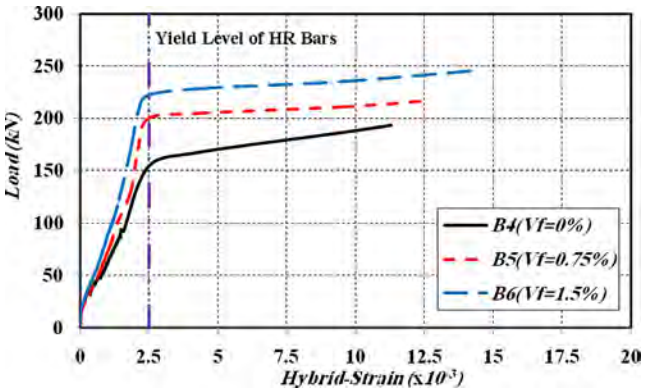

Fig. 15. Load-Hybrid Strain of the Tested Beams for Group B.

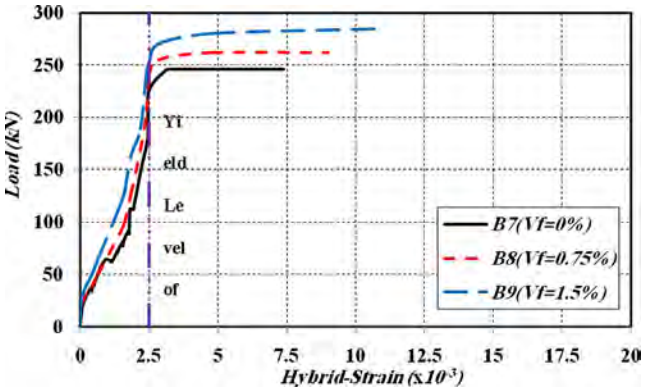

Fig. 16. Load-Hybrid Strain of the Tested Beams for Group C.

Table 7
Experimental Hybrid Strain of the Tested Beams.

Group	Beam	Strain at Yield Level, (ε_y)	Reinforcing Strain, (ε_{hr})	Strain Ductility, $\mu_s = \frac{\varepsilon_{hr}}{\varepsilon_y}$
A	**B1**	0.0025	0.0153	6.10
	B2	0.0025	0.0168	6.70
	B3	0.0025	0.0180	7.11
B	**B4**	0.0025	0.0112	4.48
	B5	0.0025	0.0127	5.08
	B6	0.0025	0.0145	5.78
C	**B7**	0.0025	0.0074	2.96
	B8	0.0025	0.0090	3.60
	B9	0.0025	0.0108	4.30
D	**B10**	0.0025	0.0048	1.90
	B11	0.0025	0.0060	2.41
	B12	0.0025	0.0070	2.81

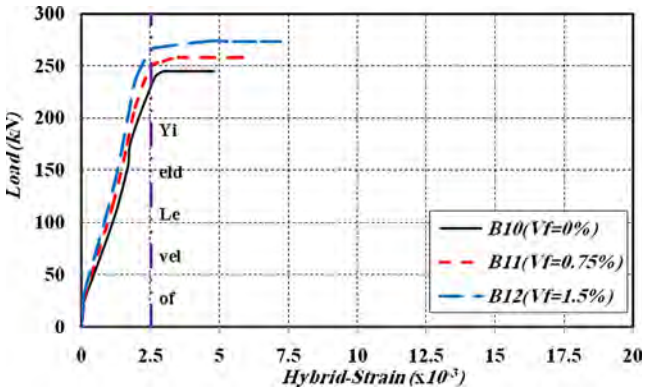

Fig. 17. Load-Hybrid Strain of the Tested Beams for Group D.

curves for Groups A, B, C, and Group D are plotted in Figs. 14–17. A close examination of the strain measurements reveals that the strain of the hybrid bars at the ultimate level (ε_{hr}) exceeds the strain at the yield level (ε_y) for all beams. Accordingly, all beams have been failed in a ductile manner in the tension zone as a consequence of the under reinforcement ratios. Based on the strain measurements, the bond failure was not observed in all the test specimens. From the load-hybrid strain curves, the strain ductility (μ_s) was defined as the ratio between strain in the hybrid bars at the ultimate level to the strain at the yield level ($\mu_s = \varepsilon_{hr} / \varepsilon_y$) [33].

Test results showed that increasing the hybrid reinforcement ratio reduced the strain ductility of the tested beams. Compared to B1, the strain ductility decreased by 20% and 50% for B4 and B7. On the other hand, the provision of PVA fibers displayed acceptable improvement in the strain ductility of the tested beams. For Group C, comparing with beam B7, the strain ductility was improved for B8 and B9 by 25% and 46%. Moreover, using hybrid schemes for concrete beams with PVA-ECC fiber showed a great efficiency to overcome the brittle behaviour of GFRP concrete beams. The ductility of beams reinforced with hybrid bars was increased with the inclusion of PVA fibers. The strain ductility of beams B11 and B12 was higher than B10 by 15% and 41% respectively. Meng et al. [20] recorded that when compared with the normal concrete matrix, the PVA matrix allows a higher strain to be developed in the tensile reinforcement bars. Furthermore, the stress distribution in the tensile reinforcement showed more uniformity for PVA concrete beams when compared to the ordinary RC beams.

3.4. Failure modes and cracks pattern

Tracing the cracks at different load levels is one of the most powerful procedures to identify the failure mechanism and highlighting the related effect of the experimental variables. The cracks pattern for Groups A, B, C, and D were the same as presented in Figs. 18–21. Generally, initial crack for all tested beams appeared in the beam mid-span at the flexural region followed by consecutive cracks away from this region in the direction of supports with increasing load increments. Increasing load values led to deeper

B1

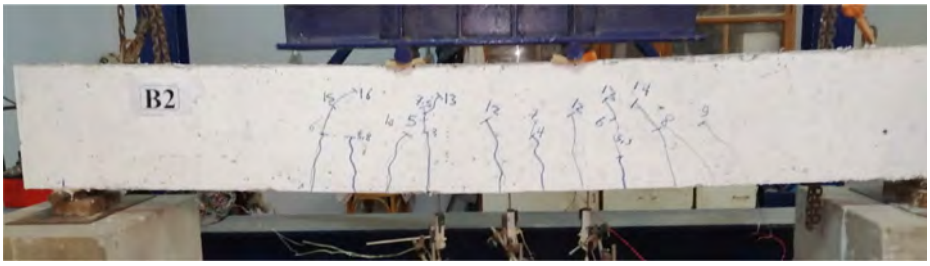

B2

B3

Fig. 18. Cracks Pattern for Group A.

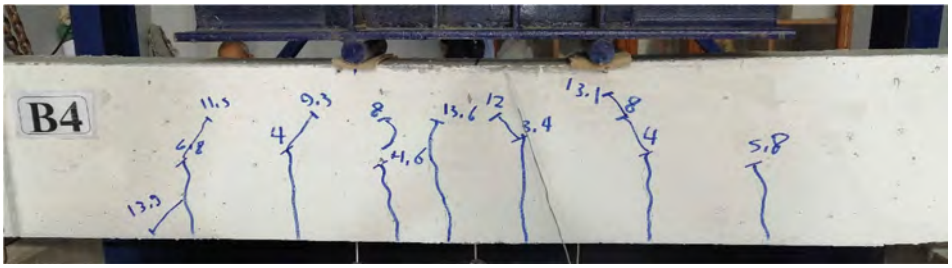

B4

B5

B6

Fig. 19. Cracks Pattern for Group B.

B7

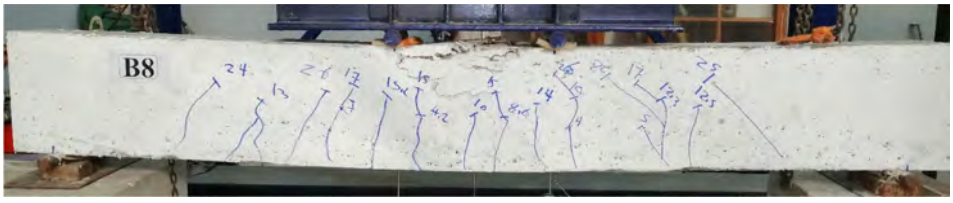

B8

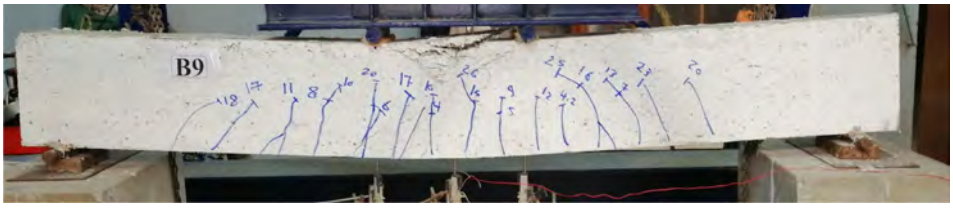

B9

Fig. 20. Cracks Pattern for Group C.

B10

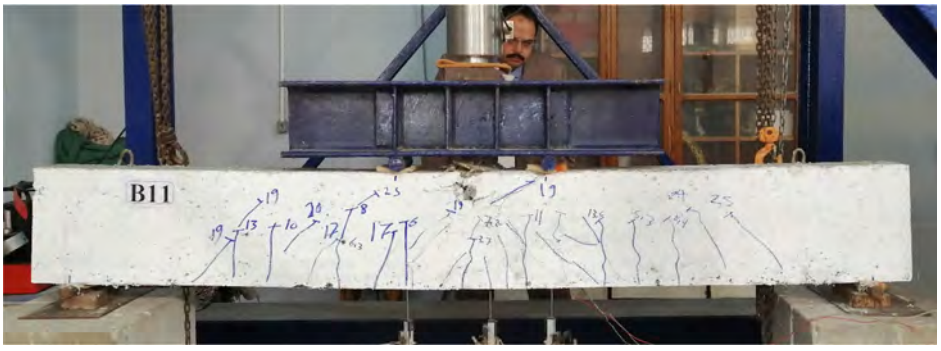

B11

B12

Fig. 21. Cracks Pattern for Group D.

and widened cracks with a major flexural crack in the maximum moment area at the failure load level. The failure type for all tested beams was recorded as a flexure failure by tensile crisis of bars.

Due to the strain hardening behaviour property of PVA fibers, this type of fibers could sustain tension load after cracking with improved the load-capacity. Using PVA fibers for the tested beams delayed the appearance of the first cracking with reference to the non-fibrous beams. Increasing the fiber content delayed the appearance of the first crack by 28% and 40% for beams B5 and B6 when compared to B4. Also, increasing the hybrid reinforcement ratios resulted in less spread cracks and less visual crack width. Moreover, using the hybrid schemes of hybrid bars with GFRP bars increased the cracking loads and reduced crack propagation. The inclusion of PVA fibers in the beams reinforced with hybrid schemes enhanced the cracking loads and decreased the propagation of cracks. The crack pattern of the tested beams recorded the same pattern of the tested beams by Shanour et al. [18].

4. Non-linear finite elements analysis (NLFEA)

NLFEA was performed to simulate the tested concrete beams. The commercially available finite element analysis software package ANSYS (ANSYS release 12.1) [50] was used. The load–deflection curve is an important aspect of verifying the behaviour of beams. It includes beneficial parameters such as: cracking loads (P_{cr}), the load at yield point (P_y), the corresponding deflection (δ_y), the ultimate load (P_u), the corresponding ultimate deflection (δ_u), and energy absorption (I). Also, the strain ductility ($\mu_{s,\ NL.}$) was predicted. Accordingly, comparing the predicted results from the idealized models with the experimental results is an efficient method to validate the models.

4.1. Finite element geometric and material idealization

The structural element types used for the geometric idealization of the different materials are Solid 65 for concrete as its capability to the plastic deformation, cracking and crushing in three directions. 3-D spar elements (Link 8) was used for idealized reinforcing bars and stirrups. It has two nodes and three DOF. Also, it has the capability of plastic deformation. Solid 45 was idealized at the location of loading and supports in the concrete beams to avoid stress concentration problems. Perfect bond was assumed between the concrete and bars. The PVA fiber reinforcements were simulated as smeared reinforcements in Solid 65 element represented through volumetric ratio to represent the actual fiber volumes used in each beam specimen. Said et al. [33] used the same ele-

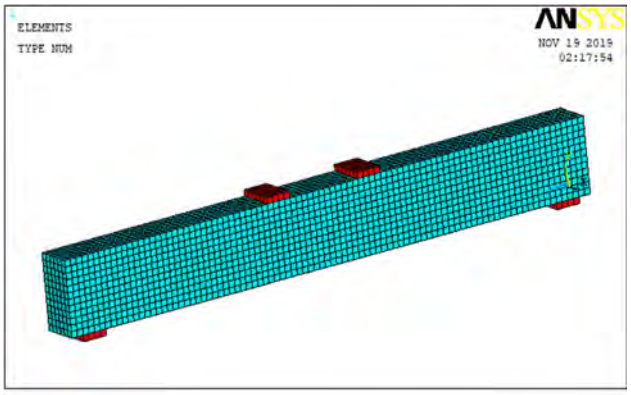

(a) Concrete Element; Solid65

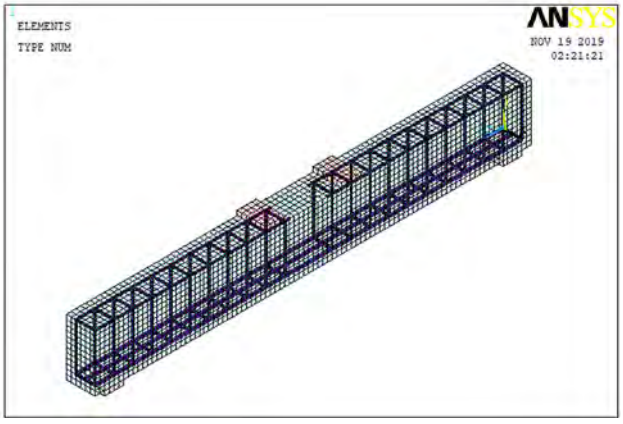

(b) Reinforcing Bar Element; Link8

Fig. 22. Finite Element Simulation Models for the Tested Beams.

ments and procedures for modelling concrete beams with GFRP bars. They get reasonable agreement comparing test results. For concrete in compression, the Hognestad-Popvics stress–strain curve [53] was used. Linear elastic behaviour was adopted for the GFRP bars. The idealized stress–strain curve for the hybrid bars shown in Fig. 4 and Eq. (1) was used in the idealization. The 3-D model for a typical beam is presented in Fig. 22.

4.2. NLFEA model verification

NLFEA results were verified with the experimental test results. First, cracks appeared at the maximum tension zone in the mid-span. Then, the cracks propagated in an upward direction through the depth of the beam. New cracks occurred in the shear region due to increasing the load, as shown in Fig. 23.

All beams showed similar patterns of crack development and propagation. NLFEA showed the first formation of vertical cracks in the mid-span at load levels of 28–42 kN. The predicted cracking loads ($P_{cr\text{-}NL.}$) were close to experimental crack loads ($P_{cr\text{-}exp.}$). The average value of the ratio ($P_{cr\text{-}exp.}$ / $P_{cr\text{-}NL.}$) is 1.07 with a standard deviation of 0.025.

4.3. Load- deflection comparison

The analytical results for all beams were very close to the experimental results. Generally, the load–deflection curves for the tested beams displayed similar features. A comparison of the load–deflection curves extracted from ANSYS and test results for all the beams are plotted in Fig. 24 and listed in Table 8. The comparison evinced that, at the yield level, the overall average ratio [$P_{y,\ exp.}$ / $P_{y,\ NL.}$] is 1.05, and the average yield deflection ratio [$\delta_{y,\ exp.}$ / $\delta_{y,\ NL.}$] is 0.97. At the ultimate level, the average ratio [$P_{u,\ exp.}$ / $P_{u,\ NL.}$] for all beams is 1.012 and the average value of deflection ratio [$\delta_{u,\ exp.}$ / $\delta_{u,\ NL.}$] is 1.01. Also, the average energy absorption ratio [$I_{exp.}$ / $I_{NL.}$] for all beams is 1.038. Moreover, the average strain ductility [$\mu_{s,\ exp.}$ / $\mu_{s,\ NL.}$] is 0.96 for all tested beams. Accordingly, the current models reasonably predicted the flexural behaviour of the PVA concrete beams reinforced with hybrid bars.

5. Flexural capacity and flexural rigidity

The strain compatibility method was performed to compare the experimental results with the nominal flexural strength ($M_{n.}$).The nominal flexural strength is estimated for a single hybrid RC rectangular beam of a cross-section ($b \times t$). The proposed equation of the current research is an enhancement equation of ACI-code 318–18 [54]. The main assumptions to predict the nominal flexural strength were considered. Moreover, the idealized stress–strain curve for the hybrid bar and the contribution of PVA fibers in the tension side were considered. Fig. 25 presents the simplified rectangular stress block considering all combinations of reinforcement steel bars, FRP bars and hybrid bars. Accordingly, the equilibrium equation can be expressed as follows:

$$C_c = T_s + T_f + T_{hr} + T_{et} \tag{2}$$

The compression force of concrete (Cc) can be estimated depending on the rectangular stress block which, calculated generally as:

$$C_c = \sigma_{ec} * A_c \tag{3}$$

The compressive strength of PVA-ECC concrete (σ_{ec}) can be defined as:

$$\sigma_{ec} = \alpha.f'_{\exp} \tag{4}$$

The coefficient (α) assumed to be 0.85, according to ACI-code 318-18 [54]. Also, the cylindrical compressive strength of the PVA-ECC concrete (f_{ecp}'). Additionally, the area of compression zone (A_c) was defined as:

$$A_c = b.a \tag{5}$$

The depth of the rectangular stress block (a) was estimated as:

$$a = \beta.C \tag{6}$$

Factor (β) should not exceed 0.85 but shall not be taken less than 0.65 [54]. It can be calculated as:

$$\beta = 0.85 - 0.05\left[\frac{f'_{ecp} - 28}{7}\right] \tag{7}$$

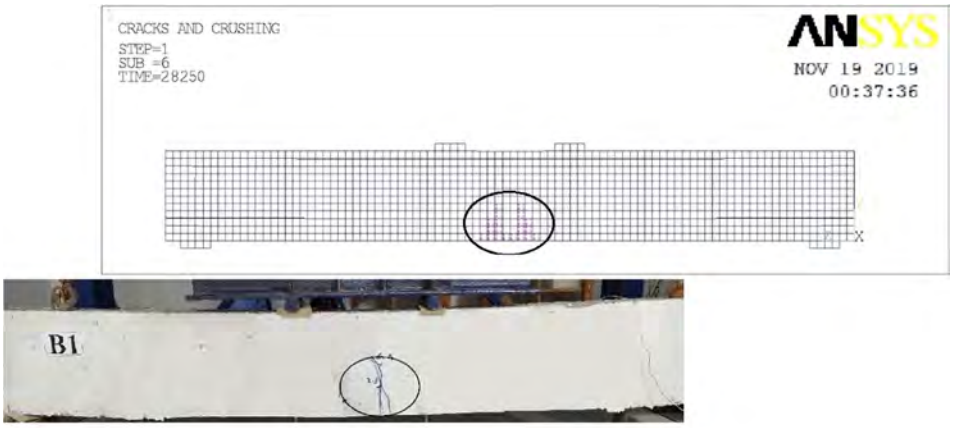

(a) At Cracking Load, P_{cr}

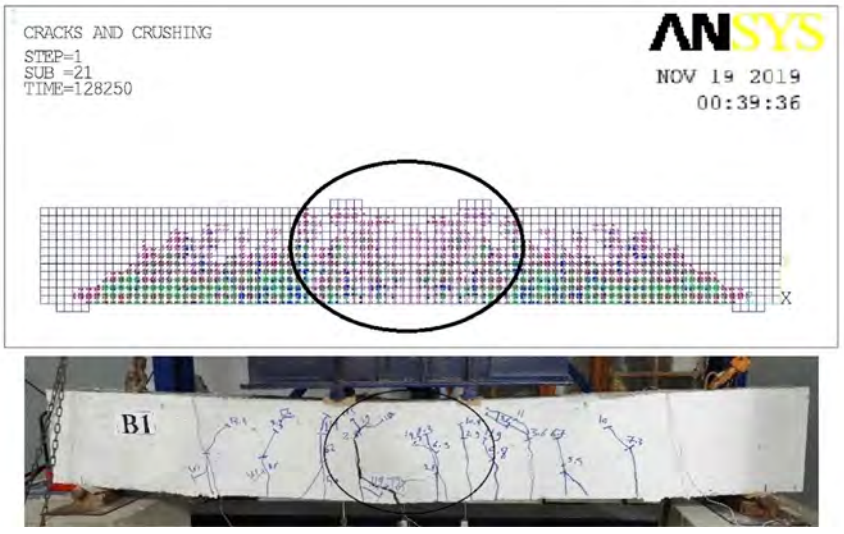

(b) At Failure

Fig. 23. Cracks Propagation for Beam B1.

Conclusively, *Cc* can be defined as:

$$C_c = 0.85 * f'_{\exp} * b * a \tag{8}$$

For under reinforced section, the tension force of reinforcing bars T_s, T_f and T_{hr} can be calculated as follows:

$$T_S = f_y * A_s \tag{9}$$

$$T_f = f_f * A_f \tag{10}$$

$$T_{hr} = f_{hr} * A_{hr} \tag{11}$$

Due to the excellent performance of PVA-ECC in tension, (T_{et}) can be estimated as follows:

$$T_{et} = \sigma_{et} * A_{et} \tag{12}$$

The area of ECC concrete in the tension side (A_{et}) can be defined as follows:

$$A_{et} = b.e \tag{13}$$

The tensile strength of PVA-ECC concrete (σ_{et}) can be predicted as [18]:

$$\sigma_{et} = 0.00772 \frac{l_f}{\varphi_f} \rho_{PVA} F_{be} \tag{14}$$

The bond efficiency of the fiber (F_{be}) varies from 1.0 to 1.2 depending upon fiber characteristics. The percent by volume of the used fibers (ρ_{PVA}) can be calculated as follows:

$$\rho_{PVA} = V_f \frac{e}{t}.100 \tag{15}$$

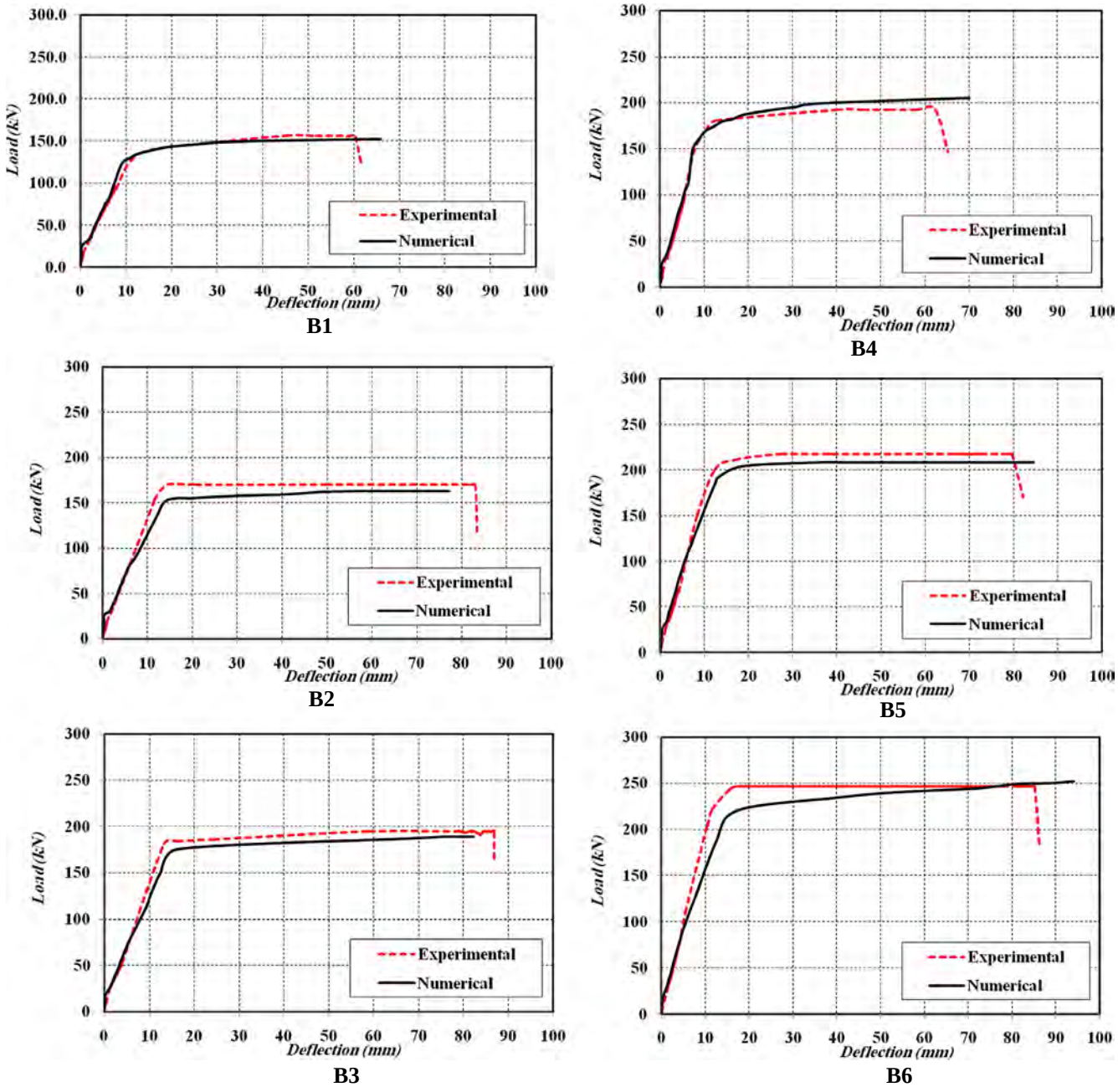

Fig. 24. Comparison of Predicted Deflections with Experimental Values.

Based on the rectangular stress block and the equilibrium equation, (a) and (C) can be predicted. Accordingly, $M_{n.}$ can be estimated as:

$$M_{n.} = \left[\left(A_s f_y + A_f f_f + A_{hr} f_{hr}\right)\left(d - \frac{a}{2}\right)\right] + \left[\sigma_{et} * b * e * \left(\frac{t+c}{2} - \frac{a}{2}\right)\right] \quad (16)$$

A simplified method for flexural rigidity (D) prediction of PVA-ECC concrete beams reinforced with hybrid bars or schemes at the yield load level is presented. The flexural rigidity at the yield load level can be defined as (D = $E\ I_{eff}$). According to the ACI 440.1R-03 [55] code, the effective moment of inertia of concrete beams (I_{eff}) up to the serviceability loading level can be defined as:

$$I_{eff} = \left(\frac{M_{cr}}{M_a}\right)^3 I_g \beta_d + \left[1 - \left(\frac{M_{cr}}{M_a}\right)^3\right] I_{cr} \quad (17)$$

The value of the applied moment (M_a) was calculated based on the measured experimental yield load and accordingly calculating the yield moment by the elastic analysis.

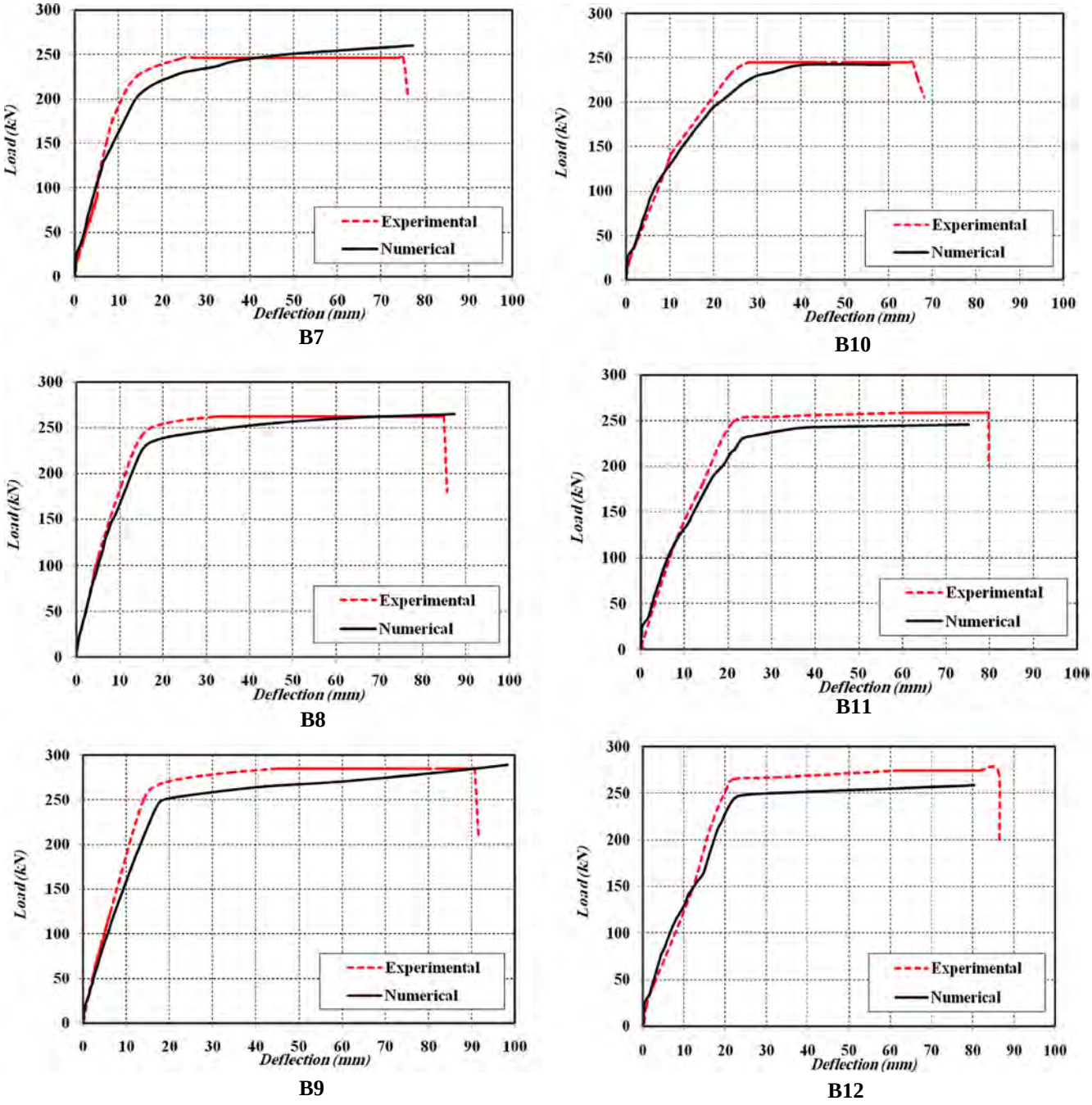

Fig. 24 (*continued*)

The flexural cracking moment (M_{cr}) is calculated as follows:

$$M_{cr} = f_{cr}\frac{I_g}{y_t} \tag{18}$$

The rupture modulus of concrete (f_{cr}) is defined according to ACI 318-18 [54] as:

$$f_{cr} = 0.62\sqrt{f'_c} \tag{19}$$

The depth of the neutral axis measured from the tension side (y_t) as shown in Fig. 26, can be calculated as:

$$y_t = \frac{\left(\frac{bt^2}{2}\right) + \left[(n_s - 1)A_s + (n_f - 1)A_f + (n_{hr} - 1)A_{hr}\right]d'}{A_t} \tag{20}$$

The modular ratios of reinforcing steel bars (n_s), GFRP bars (n_f), and hybrid bars (n_{hr}) were defined as (E_s/E_c), (E_f/E_c), and (E_{hr}/E_c)

Table 8
Comparison of Experimental Results with NLFEA Results.

Beam	Experimental Results						NLFEA Results							Experimental Results/ NLFEA Results								
	P_{cr} (kN)	P_y (kN)	δ_y (mm)	P_u (kN)	δ_u (mm)	K (kN/mm)	I (kN.mm)	DF	μ_s	P_{cr} (kN)	P_y (kN)	δ_y (mm)	P_u (kN)	δ_u (mm)	K (kN/mm)	I (kN.mm)	DF	μ_s	$\frac{P_{cr\text{-}exp.}}{P_{cr\text{-}NL}}$	$\frac{P_{y\text{-}exp.}}{P_{y\text{-}NL}}$	$\frac{\delta_{y\text{-}exp.}}{\delta_{y\text{-}NL}}$	$\frac{P_{u\text{-}exp.}}{P_{u\text{-}NL}}$	$\frac{\delta_{u\text{-}exp.}}{\delta_{u\text{-}NL}}$	$\frac{K_{exp.}}{K_{NL}}$	$\frac{I_{exp.}}{I_{NL}}$	$\frac{DF_{exp.}}{DF_{NL}}$	$\frac{\mu_{s\,exp.}}{\mu_{s\,NL}}$
B1	29	135	10	157	61	13.5	8300	6.10	6.10	28	122	10.98	150.1	66.1	12.30	8420	6.02	6.35	1.04	1.11	0.91	1.05	0.92	1.10	0.99	1.01	0.95
B2	33	154.5	11.3	170	83	13.67	13,115	7.35	6.70	32	151	12.4	163	77.0	12.18	11,900	6.21	6.88	1.03	1.02	0.91	1.04	1.08	1.12	1.10	1.18	0.97
B3	40	181	11.89	195	88	15.22	15,500	7.40	7.11	37	171	13	189	82.0	13.15	14,200	6.31	7.52	1.08	1.06	0.91	1.03	1.07	1.16	1.09	1.17	0.94
B4	32	155	9	193	67	17.2	11,800	7.44	4.48	30	150	8.6	200	68	17.44	12,600	7.91	5.04	1.07	1.03	1.05	0.97	0.99	0.99	0.94	0.94	0.89
B5	41	200	10.5	217	82	19.05	16,400	7.81	5.08	38.5	190	10.6	208	84.0	17.92	16,300	7.92	5.32	1.06	1.05	0.99	1.04	0.98	1.06	1.01	0.99	0.95
B6	45	222	11	246	86	20.18	19,600	7.82	5.78	42	218	11.8	252	94.0	18.47	19,500	7.97	5.92	1.07	1.02	0.93	0.98	0.91	1.09	1.01	0.98	0.97
B7	34	220	12	246	73	18.3	16,900	6.28	2.96	32	204	11	260	77.3	18.4	17,150	7.02	3.06	1.06	1.08	1.09	0.95	0.94	1.00	0.99	0.89	0.96
B8	42	240	13	261	84	18.46	20,418	6.462	3.60	39	229	12.7	265	87.3	18.03	20,312	6.87	3.84	1.08	1.05	1.02	0.98	0.96	1.02	1.01	0.94	0.93
B9	46	252	13.5	285	90	18.67	23,600	6.667	4.30	41	250	15	289	98.0	16.67	24,255	6.53	4.48	1.12	1.01	0.90	0.99	0.92	1.12	0.97	1.02	0.96
B10	35	230	23	245	66	10.0	14,100	2.87	1.90	32.0	220	20.0	243.3	60.5	10.0	12,500	3.0	1.96	1.09	1.05	1.15	1.01	1.09	1.00	1.13	0.95	0.97
B11	37	248	20	258	80	12.40	17,900	4.00	2.41	34	234	21.25	245	75.0	11.01	15,800	3.53	2.24	1.09	1.06	0.94	1.05	1.07	1.13	1.13	1.13	1.07
B12	40	265	20	273	86	13.25	20,600	4.30	2.81	38	240	22	258	80.0	10.91	18,700	3.64	2.78	1.05	1.10	0.91	1.06	1.08	1.21	1.10	1.18	1.01
Average																			**1.071**	**1.053**	**0.977**	**1.012**	**1.01**	**1.083**	**1.038**	**1.033**	**0.96**
Standard deviation																			**0.025**	**0.031**	**0.083**	**0.039**	**0.071**	**0.071**	**0.068**	**0.106**	**0.04**
Coefficient of variation																			**2.33%**	**2.97%**	**8.54%**	**3.83%**	**7.06%**	**6.55%**	**6.58%**	**10.2%**	**4.5%**

respectively. Also, the total cross-section area of the beam (A_t) is calculated as follows:

$$A_t = (b.t) + (n_s - 1)A_s + (n_f - 1)A_f + (n_{hr} - 1)A_{hr} \quad (21)$$

Accordingly, the gross moment of inertia (I_g) can be obtained as:

$$I_g = \left[\frac{bt^3}{12} + bt\left(\frac{t}{2} - y_t\right)^2\right] + \left[(n_s - 1)A_s + (n_f - 1)A_f + (n_{hr} - 1)A_{hr}\right](y_t - d')^2 \quad (22)$$

The parameter (β_d) is accounted for the bond properties and elastic modulus of FRP bars, it is defined by ACI 440.1R-03 [55] as follows:

$$\beta_d = 0.5\left[\frac{E_f}{E_s} + 1\right] \quad (23)$$

To predict the cracked moment of inertia (I_{cr}). The depth of the compression zone (Z) measured from the neutral axis should be calculated. Fig. 27 shows the contribution of the tensile reinforcement bars and PVA-ECC fiber in the tension zone. Accordingly, Z can be calculated as:

$$\frac{bZ^2}{2} = \left[(n_sA_s + n_fA_f + n_{hr}A_{hr})(d - Z)\right] + m\sigma_{et}b(d - Z) \quad (24)$$

σ_{et} is predicted from Eq. (14) and m is the modular ratio of PVA = (E_{PVA} / E_c). Accordingly, the cracked moment of inertia (I_{cr}) can be calculated as:

$$I_{cr} = \left(\frac{bt^3}{3}\right) + \left[n_sA_s + n_fA_f + n_{hr}A_{hr}\right](d - Z)^2 + m\sigma_{et}(d - Z)^2 \quad (25)$$

Based on the previous equations, the effective moment of inertia (I_{eff}) and the flexural rigidity (D) at the yield level could be predicted. The analysis procedure for calculating $M_{n.}$ and I_{eff} can be easily implemented by hand calculations or a spreadsheet. $M_{n.}$ and I_{eff} were calculated for all tested beams using Eq. (16) and Eq. (17) respectively. The experimental value of the moment of inertia ($I_{eff,\ exp.}$) was calculated based on the measured yield load ($P_{y,\ exp.}$) and the corresponding displacement ($\delta_{y,\ exp.}$). Accordingly, for the four-point bending beam, $I_{eff,\ exp.}$ was calculated as follows [54]:

$$I_{eff,exp.} = \frac{P_{y,exp.}X}{48E_c\delta_{y,exp.}}(3L^2 - 4X^2) \quad (26)$$

Table 9 presents a comparison between the experimental and nominal flexural strength. It concluded that good agreements between the experimental and the nominal flexural strength were achieved. The average ratio of [$M_{u,\ exp.}$ / $M_{n.}$] for the tested beams is 1.04. Also, the average ratio of [$I_{eff,\ exp.}$ / $I_{eff,\ n.}$] for the tested beams is 1.05 with 0.07 standard deviation and the coefficient of variation equals 6.8%. Moreover, Table 9 includes a comparison with 77 ECC concrete beams reinforced with hybrid bars previously tested by [18,20–21,34–35,41]. The nominal flexural strength and the flexural rigidity generally performs well in predicting the flexural strength. The overall average value of the ratio [$M_{u,\ exp.}$ / $M_{n.}$] is 1.015 with a standard deviation of 0.085 and the coefficient of variation equals 8.5%. Also, the overall average value of the ratio [$I_{eff,\ exp.}$ / $I_{eff,\ n.}$] is 1.03 with a standard deviation of 0.087.

Using the flexural rigidity predictions at the yield level, sensitivity studies are performed to investigate the effect of fiber content (V_f) on the ratio between the flexural rigidity for PVA-ECC beams ($D_{,\ ECC}$) and the flexural rigidity for RC beams ($D_{,RC}$) at the yield level. From Fig. 28, it can be concluded that the flexural capacity of PVA-ECC beams ($D_{,\ ECC}$) is improved by increasing fiber volume (V_f). Considering the constant (ρ_{hr}) ratio as 0.85, the increase of

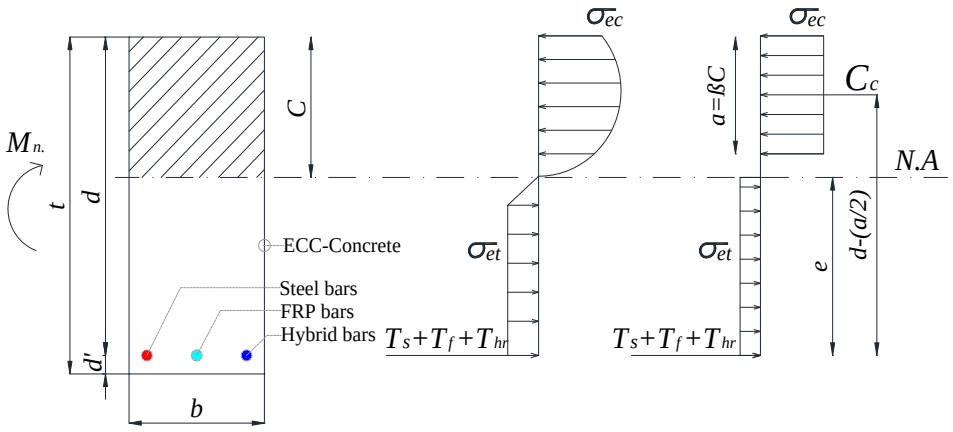

(a) General Cross Section (b) Stress Distribution (c) Rectangle Stress Block

Fig. 25. Cross Section Stress Distribution for PVA-ECC Concrete Beams.

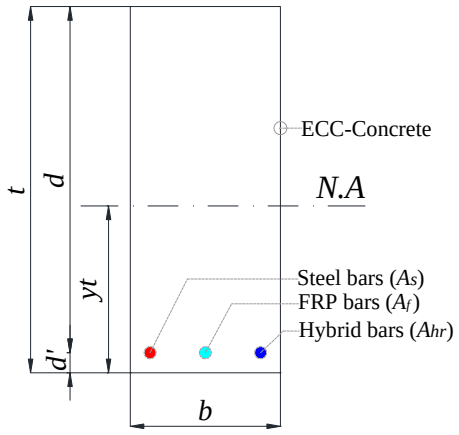

Fig. 26. Calculation of y_t.

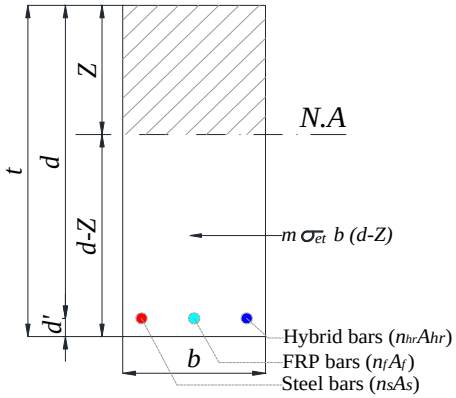

Fig. 27. Compression Zone Prediction.

(V_f) from 0.0 to 1.5% enhances the $D_{,\ ECC}$ by 30%. As presented in Fig. 29, increasing the hybrid reinforcement ratio (ρ_{hr}) showed significant enhancement in the flexural rigidity at the yield level of PVA-ECC beams. Keeping the fiber volume (V_f) as 1.5%, increasing ρ_{hr} from 0.85% for B3 to 1.7% improved the flexural rigidity for B9 (hybrid bars) and B12 (hybrid schemes) by 63% and 40% respectively. Accordingly, using the hybrid bars in reinforcing PVA-ECC beams are more effective than the hybrid schemes bars.

6. Conclusions

The flexural behaviour of PVA-ECC concrete beams reinforced with locally produced hybrid bars was investigated. Based on the experimental results and the comparison with the NLFEA and predicted nominal flexural strength in this study, the following conclusions can be drawn:

1) Generally, the provision of PVA fibers exhibits an enhancement in the cracking load and the load-carrying capacity of the tested beams. The enhancement in the ultimate capacity was 12% and 27% for the PVA ratio of 0.75% and 1.5%. The increase in the load-carrying capacities using PVA-ECC material can be illustrated by the strain hardening and multiple micro-cracking behaviours.
2) The inclusion of the hybrid bars enhanced the cracking load, ultimate capacity, ductility factor, and energy absorption of test beams. The enhancement in the ultimate capacity was 23% and 57% for B4 and B7 regarding B1. Also, the improvement in energy absorption was 50% and 104% for B4 and B7.
3) Increasing PVA-ECC content delayed the appearance of the first crack of the tested beams. Increasing the PVA ratio delayed the appearance of the first crack by 14% and 38% for beams B2 and B3. Moreover, at failure load, less spread cracks and less visual crack width was observed.
4) PVA fibers allow a higher strain to be developed in the hybrid bars. Increasing the PVA content improved the strain ductility of the hybrid bars by 25% and 46% for B8 and B9 regarding B7.
5) According to the results of tested specimens, the hybrid schemes showed a change in the failure mode from compression failure to tension failure, which indicated more ductile behaviour for the beams. Also, bond failure was not observed for the tested beams.
6) The application of NLFEA to the tested beams yielded acceptable load-carrying capacities and load–deflection curves. The analysis adequately reflected the trend of experimental results. At the ultimate level, the overall average ratio [$P_{u,\ exp.}$ / $P_{u,\ NL.}$] was 1.012 with a standard deviation of 0.04, and the coefficient of variation equal to 3.8%.

Table 9
Experimental and Nominal Flexural Strength.

Author	Beam	f_c'	Geometrical Parameters				Bottom RFT							PVA-ECC Parameters				$M_{exp.}$ (kN.m)	$I_{eff,\ exp.}$ (mm^4)	$M_{n.}$ (kN.m)	$I_{eff,\ n.}$ (mm^4)	$\frac{M_{exp.}}{M_{n.}}$	$\frac{I_{eff\ exp.}}{I_{eff\ n.}}$
		MPa	b (mm)	d (mm)	$L_{CL\text{-}CL}$ (mm)	X (mm)	A_s HTS	f_y MPa	A_f FRP	f_f MPa	A_{hr} HR	f_{hr} HR	ρ_t %	Vf (%)	l_f (mm)	ϕ_f (mm)	e (mm)						
Present	**B1**	46.5	150	275	2100	850	–	–	–	–	2H14	630	0.85	–	–	–	–	66.725	101940972	60	95060082	1.11	1.07
	B2	48	150	275	2100	850	–	–	–	–	2H14	630	0.85	0.75	12	0.039	300	72.25	110381944	67	109688629	1.08	1.01
	B3	50	150	275	2100	850	–	–	–	–	2H14	630	0.85	1.5	12	0.039	300	82.875	126614583	75	125397440	1.11	1.01
	B4	46.5	150	275	2100	850	–	–	–	–	3H14	630	1.26	–	–	–	–	82.025	125315972	82	131002391	0.99	0.96
	B5	48	150	275	2100	850	–	–	–	–	3H14	630	1.26	0.75	12	0.039	300	92.225	140899305	90	142781941	1.02	0.99
	B6	50	150	275	2100	850	–	–	–	–	3H14	630	1.26	1.5	12	0.039	300	104.55	159729166	98	156965340	1.06	1.02
	B7	46.5	150	275	2100	850	–	–	–	–	4H14	630	1.7	–	–	–	–	104.55	150225281	102	154889358	1.02	0.97
	B8	48	150	275	2100	850	–	–	–	–	4H14	630	1.7	0.75	12	0.039	300	110.925	169468750	112	172725492	0.99	0.98
	B9	50	150	275	2100	850	–	–	–	–	4H14	630	1.7	1.5	12	0.039	300	121.125	190640656	118	185657788	1.03	1.03
	B10	46.5	150	275	2100	850	–	–	3G12	850	2H14	630	1.7	–	–	–	–	104.125	159079861	102	134279848	1.02	1.18
	B11	48	150	275	2100	850	–	–	3G12	850	2H14	630	1.7	0.75	12	0.039	300	109.65	167520833	109	147233170	1.01	1.14
	B12	50	150	275	2100	850	–	–	3G12	850	2H14	630	1.7	1.5	12	0.039	300	116.025	177260416	115	162323799	1.01	1.09
Shanour, et al. [18]	**B1**	44	115	255	1650	650	2ϕ16	400	–	–	–	–	1.37	–	–	–	–	37.4	82999725	38.01	89031618	0.98	0.93
	B2	44	115	255	1650	650	2ϕ16	400	–	–	–	–	1.37	1	12	0.039	280	44.9	87532817	45.52	93609841	0.99	0.94
	B3	44	115	255	1650	650	2ϕ16	400	–	–	–	–	1.37	2	12	0.039	280	50.1	92612847	52.15	98421146	0.96	0.94
	B4	44	115	255	1650	650	2ϕ16	400	–	–	–	–	1.37	0.5	12	0.039	280	41.3	76025843	46.50	81982665	0.89	0.93
	B5	44	115	255	1650	650	2ϕ16	400	–	–	–	–	1.37	1	12	0.039	280	46.5	89794303	52.00	94214341	0.89	0.95
	B6	44	115	255	1650	650	2ϕ16	400	–	–	–	–	1.37	2	12	0.039	100	46.8	70338871	42.45	77613915	1.10	0.91
	B7	44	115	255	1650	650	2ϕ16	400	–	–	–	–	1.37	1	12	0.039	200	45.2	71745648	52.08	79328197	0.87	0.90
	B8	44	115	255	1650	650	2ϕ12	400	–	–	–	–	0.77	–	–	–	–	26.3	52865214	22.12	54961342	1.19	0.96
	B9	44	115	255	1650	650	2ϕ12	400	–	–	–	–	0.77	0.5	12	0.039	100	28.9	63853627	25.48	59494803	1.13	1.07
	B10	44	115	255	1650	650	2ϕ12	400	–	–	–	–	0.77	1	12	0.039	100	32.8	64492163	28.78	59494803	1.14	1.08
	B11	44	115	255	1650	650	2ϕ12	400	–	–	–	–	0.77	0.5	12	0.039	200	31.2	59084651	30.38	58286792	1.03	1.01
	B12	44	115	255	1650	650	2ϕ12	400	–	–	–	–	0.77	1	12	0.039	200	35.4	67525316	37.96	62554472	0.93	1.08
Meng, et al. [20]	**B1**	45	100	180	1800	600	2ϕ12	400	–	–	–	–	1.26	–	–	–	–	16.25	28137428	15.22	27935619	1.07	1.01
	B2	47	100	180	1800	600	2ϕ12	400	–	–	–	–	1.26	2.2	12	0.039	200	21.4	28723625	21.21	30024143	1.01	0.96
	B3	49.8	100	180	1800	600	2ϕ12	400	–	–	–	–	1.26	–	–	–	–	16.25	28137428	15.32	27935619	1.06	1.01
	B4	51.9	100	180	1800	600	2ϕ12	400	–	–	–	–	1.26	2.2	12	0.039	200	21.2	28723625	21.61	30024143	0.98	0.96
Alyousif, et al. [21]	**B1**	49	125	215	830	215	2ϕ16	520	–	–	–	–	1.50	1.5	8	0.039	250	52.4	52747843	47.29	59888227	1.11	0.88
	B2	49	125	190	780	190	4ϕ16	520	–	–	–	–	3.39	1.5	8	0.039	250	54	42279429	53.40	45166629	1.01	0.94
	B3	49	125	215	1260	430	2ϕ16	520	–	–	–	–	1.50	1.5	8	0.039	250	47.5	48860541	47.29	47947523	1.00	1.02
	B4	49	125	190	1160	380	4ϕ16	520	–	–	–	–	3.39	1.5	8	0.039	250	55.5	53387716	56.70	54970587	0.98	0.97
	B5	49	125	215	1690	645	2ϕ16	520	–	–	–	–	1.50	1.5	8	0.039	250	47	52005836	47.29	57282472	0.99	0.91
	B6	49	125	190	1540	570	4ϕ16	520	–	–	–	–	3.39	1.5	8	0.039	250	55	60638701	56.70	68713234	0.97	0.88
	B7	54.9	125	215	830	215	2ϕ16	520	–	–	–	–	1.50	–	–	–	–	41	48045107	39.39	49991661	1.04	0.96
	B8	54.9	125	190	780	190	4ϕ16	520	–	–	–	–	3.39	–	–	–	–	46	37694657	53.40	34973807	0.86	1.08
	B9	54.9	125	215	1260	430	2ϕ16	520	–	–	–	–	1.50	–	–	–	–	42	43796429	39.39	42853125	1.07	1.02
	B10	54.9	125	190	1160	380	4ϕ16	520	–	–	–	–	3.39	–	–	–	–	48	40782283	53.40	39533855	0.90	1.03
Jie, et al. [34]	**HB1**	30	150	175	1400	500	2ϕ12	408	–	–	–	–	0.86	–	–	–	–	19.3	36901600	15.53	34230306	1.24	1.08
	HB2	31.4	150	175	1400	500	2ϕ12	408	–	–	–	–	0.86	2	12	0.039	51	19.5	37284000	17.22	36422303	1.13	1.02
	HB3	31.4	150	175	1400	500	2ϕ12	408	–	–	–	–	0.86	2	12	0.039	100	19.8	37857600	20.00	41914183	0.99	0.90
	HB4	31.4	150	175	1400	500	2ϕ12	408	–	–	–	–	0.86	2	12	0.039	200	22.5	43020000	24.46	45545939	0.92	0.94
	HC1	30	150	175	1400	500	2ϕ12	340	1G8	1250	–	–	1.053	–	–	–	–	22	48073142	20.78	41645450	1.06	1.15
	HC2	31.4	150	175	1400	500	2ϕ12	340	1G8	1250	–	–	1.053	2	12	0.039	51	23.9	45696800	21.81	46665498	1.10	0.98
	HC3	31.4	150	175	1400	500	2ϕ12	340	1G8	1250	–	–	1.053	2	12	0.039	100	25.7	46798476	24.25	46215171	1.06	1.01
	HC4	31.4	150	175	1400	500	2ϕ12	340	1G8	1250	–	–	1.053	2	12	0.039	200	25.4	43168711	28.45	47161505	0.89	0.92
	HD1	30	150	175	1400	500	1ϕ10	400	2G8	1250	–	–	0.682	–	–	–	–	18.3	29158000	18.96	25051952	0.97	1.16
	HD2	31.4	150	175	1400	500	1ϕ10	400	2G8	1250	–	–	0.682	2	12	0.039	51	18.6	29636000	19.92	28023232	0.93	1.06
Jie, et al. [34]	**HD3**	31.4	150	175	1400	500	1ϕ10	400	2G8	1250	–	–	0.682	2	12	0.039	100	22	35053333	23.42	32741143	0.94	1.07

(*continued on next page*)

Table 9 (*continued*)

Author	Beam	f'_c	Geometrical Parameters				Bottom RFT							PVA-ECC Parameters				$M_{exp.}$ (kN.m)	$I_{eff,\ exp.}$ (mm^4)	$M_{n.}$ (kN.m)	$I_{eff,\ n.}$ (mm^4)	$\frac{M_{exp.}}{M_{n.}}$	$\frac{I_{eff\ exp.}}{I_{eff\ n.}}$
		MPa	b (mm)	d (mm)	L_{CL-CL} (mm)	X (mm)	A_s HTS	f_y MPa	A_f FRP	f_f MPa	A_{hr} HR	f_{hr} HR	ρ_t %	Vf (%)	l_f (mm)	ϕ_f (mm)	e (mm)						
	HD4	31.4	150	175	1400	500	1ϕ10	400	2G8	1250	–	–	0.682	2	12	0.039	200	21.9	37336580	26.27	39880702	0.83	0.94
	HE1	30	150	175	1400	500	2ϕ12	400	2G8	1250	–	–	0.814	–	–	–	–	21.2	38604190	21.47	32783574	0.99	1.18
	HE2	31.4	150	175	1400	500	2ϕ12	400	2G8	1250	–	–	0.814	2	12	0.039	51	23.6	45123200	23.53	40707879	1.00	1.11
	HE3	31.4	150	175	1400	500	2ϕ12	400	2G8	1250	–	–	0.814	2	12	0.039	100	26.8	45548088	26.69	43779325	1.00	1.04
	HE4	31.4	150	175	1400	500	2ϕ12	400	2G8	1250	–	–	0.814	2	12	0.039	200	27.5	52580000	28.82	50121807	0.95	1.05
	HF1	30	150	175	1400	500	2ϕ10	400	1G8	1250	–	–	0.790	–	–	–	–	17.3	40710892	17.27	34661763	1.00	1.17
	HF2	31.4	150	175	1400	500	2ϕ10	400	1G8	1250	–	–	0.790	2	12	0.039	51	20.1	43921371	19.36	36980183	1.04	1.19
	HF3	31.4	150	175	1400	500	2ϕ10	400	1G8	1250	–	–	0.790	2	12	0.039	100	21.4	46762057	22.20	41147604	0.96	1.14
	HF4	31.4	150	175	1400	500	2ϕ10	400	1G8	1250	–	–	0.790	2	12	0.039	200	19.7	43047314	24.31	47166717	0.81	0.91
	HG1	30	150	175	1400	500	2ϕ12	400	1G8	1250	–	–	1.053	–	–	–	–	24.3	46461600	22.01	41166292	1.10	1.13
	HG2	31.4	150	175	1400	500	2ϕ12	400	1G8	1250	–	–	1.053	2	12	0.039	51	28.3	43287680	24.40	45329761	1.16	0.95
	HG3	31.4	150	175	1400	500	2ϕ12	400	1G8	1250	–	–	1.053	2	12	0.039	100	25.1	47991200	25.34	49143577	0.99	0.98
	HG4	31.4	150	175	1400	500	2ϕ12	400	1G8	1250	–	–	1.053	2	12	0.039	200	27.1	47104727	29.29	50326278	0.93	0.94
	HH1	30	150	175	1400	500	2ϕ12	500	1G8	1250	–	–	1.053	–	–	–	–	26.6	46235636	25.04	39368613	1.06	1.17
	HH2	31.4	150	175	1400	500	2ϕ12	500	1G8	1250	–	–	1.053	2	12	0.039	51	28.8	48947200	28.78	43623842	1.00	1.12
	HH3	31.4	150	175	1400	500	2ϕ12	500	1G8	1250	–	–	1.053	2	12	0.039	100	28.7	48777244	28.92	47516482	0.99	1.03
	HH4	31.4	150	175	1400	500	2ϕ12	500	1G8	1250	–	–	1.053	2	12	0.039	200	27.2	49529904	30.54	51400993	0.89	0.96
	HK1	30	150	175	1400	500	–	–	3G8	1250	–	–	0.574	–	–	–	–	17.8	8007905	16.48	7854528	1.08	1.02
	HK2	31.4	150	175	1400	500	–	–	3G8	1250	–	–	0.574	2	12	0.039	51	20.4	9177600	20.85	9909449	0.98	0.93
	HK3	31.4	150	175	1400	500	–	–	3G8	1250	–	–	0.574	2	12	0.039	100	22.3	12038851	22.22	13159664	1.00	0.91
	HK4	31.4	150	175	1400	500	–	–	3G8	1250	–	–	0.574	2	12	0.039	200	22	12787456	21.01	14382966	1.05	0.89
Qu, et al. [35]	**B1**	22.5	180	220	1800	600	4ϕ12	363	–	–	–	–	1.14	–	–	–	–	32.37	114695742	31.9	118117224	1.01	0.97
	B2	22.5	180	220	1800	600	–	–	4G12	782	–	–	1.14	–	–	–	–	43.89	139962821	40.2	138979420	1.09	1.01
	B3	22.5	180	220	1800	600	2ϕ12	363	2G12	782	–	–	1.14	–	–	–	–	38.28	105235204	41.2	97733577	0.93	1.08
	B4	22.5	180	220	1800	600	1ϕ16	336	2G16	755	–	–	1.52	–	–	–	–	39.66	97287370	42.5	86179416	0.93	1.13
	B5	22.5	180	220	1800	600	2ϕ16	336	2G10	778	–	–	1.41	–	–	–	–	36.36	115950061	39.8	120295884	0.91	0.96
	B6	22.5	180	220	1800	600	2ϕ16	336	2G12	782	–	–	1.58	–	–	–	–	42.57	135753413	45.01	127123940	0.95	1.07
	B7	22.5	180	220	1800	600	1ϕ10	363	2G10	778	–	–	0.6	–	–	–	–	23.55	68272425	22.8	62994534	1.03	1.08
	B8	22.5	180	220	1800	600	6ϕ16	336	2G16	755	–	–	4.05	–	–	–	–	63.3	240964700	66.5	225851237	0.95	1.07
Lau, et al. [41]	**B1**	39	280	355	4200	2100	–	–	4G16	593	–	–	0.81	–	–	–	–	158.8	182857946	152.52	162692342	1.04	1.12
	B2	41.3	280	355	4200	2100	–	–	4G25	528	–	–	1.98	–	–	–	–	238	269489009	218.21	243122414	1.09	1.11
	B3	42.3	280	355	4200	2100	–	–	3G12	603	–	–	0.34	–	–	–	–	79.5	135027581	68.09	116743877	1.17	1.16
	B4	42.5	280	355	4200	2100	–	–	4G25	603	–	–	0.46	–	–	–	–	107	171044927	89.97	147791836	1.19	1.16
	B5	34	280	355	4200	2100	–	–	1G25	205	–	–	0.49	–	–	–	–	220	695183687	200.05	582747879	1.10	1.19
	B6	40	280	355	4200	2100	2ϕ25	336	1G20	588	–	–	1.27	–	–	–	–	150	509538043	153.18	537996408	0.98	0.95
	B7	39.3	280	355	4200	2100	2ϕ20	579	2G25	582	–	–	1.62	–	–	–	–	261	838236403	255.85	751640036	1.02	1.12
	B8	40	280	355	4200	2100	2ϕ25	550	2G20	558	–	–	1.56	–	–	–	–	229	1037192995	252.20	985333345	0.91	1.05
	B9	39	280	355	4200	2100	4ϕ20	340	–	–	–	–	1.26	–	–	–	–	147.4	1540634002	141.84	132770533	1.04	1.16
	B10	45.9	280	355	4200	2100	4ϕ25	340	–	–	–	–	1.98	–	–	–	–	250	1715616308	216.60	157836700	1.15	1.09
	B11	35.3	280	355	4200	2100	2ϕ12	507	–	–	–	–	0.23	–	–	–	–	44	65698678	39.93	58471823	1.10	1.12
Number of Specimens																						**89**	**89**
Average																						**1.015**	**1.027**
Standard deviation																						**0.084**	**0.087**
Coefficient of variation																						**8.29%**	**8.46%**

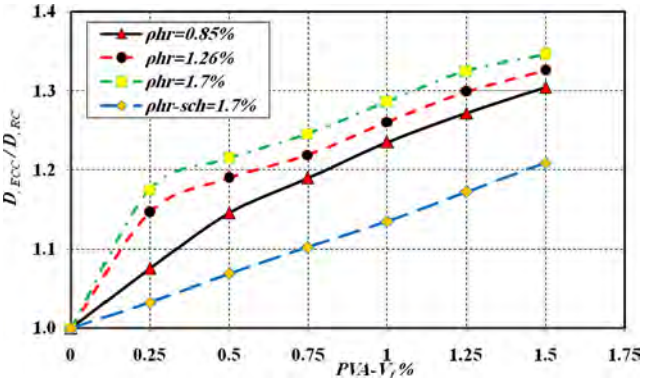

Fig. 28. Effect of PVA-Fiber Volume (V_f) on the Flexural Rigidity.

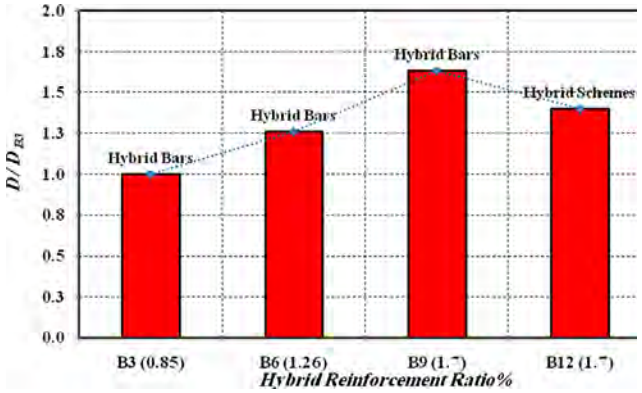

Fig. 29. Effect of Hybrid Reinforcement ratio on the Flexural Rigidity.

7) The nominal flexural strength and flexural rigidity for ECC-concrete beams reinforced with hybrid bars prove to be a successful analytical tool for predicting the flexure performance. The nominal flexure strength and flexural rigidity predictions for 89 experimental test results were on the safe side and showed consistent predictions. The overall average value of the ratio [$M_{u,\ exp.}$ / $M_{n.}$] is 1.015, with a standard deviation of 0.084, and the coefficient of variation equals 8%.
8) The sensitivity studies of the proposed model indicate that flexural rigidity for ECC concrete beams is improved by increasing fiber volume (V_f). Comparing with the non-fibrous concrete beam, the increase of (V_f) to 1.5% enhances the flexural rigidity by 30%.

Based on this investigation, consideration should be given to the feasibility and plausible future of the novel hybrid bars and PVA fibers especially for marine and waterfront RC structures.

Declaration of Competing Interest

The authors declare that they have no known competing financial interests or personal relationships that could have appeared to influence the work reported in this paper.

References

[1] I. Ray, Z. Gong, J.F. Davalos, A. Kar, Shrinkage and cracking studies of high performance concrete for bridge decks, Constr. Build. Mater. 28 (1) (2012) 244–254.
[2] J. Salimi, A.M. Ramezanianpour, M.J. Moradi, Studying the effect of low reactivity metakaolin on free and restrained shrinkage of high performance concrete, J. Build. Eng. 28 (2020) 101053, https://doi.org/10.1016/j.jobe.2019.101053.
[3] X. Qian, L. Zongjin, The relationships between stress and strain for high-performance concrete with Metakaolin, Cem. Concr. Res. 31 (2001) 1607–1611.
[4] Y. Zhu, Y. Zhang, H.H. Hussein, G. Chen, Flexural strengthening of reinforced concrete beams or slabs using ultra-high performance concrete (UHPC): a state of the art review, Eng. Struct. 205 (2020) 110035, https://doi.org/10.1016/j.engstruct.2019.110035.
[5] K.M. Liew, A. Akbar, The recent progress of recycled steel fiber reinforced concrete, Constr. Build. Mater. 232 (2020) 117232, https://doi.org/10.1016/j.conbuildmat.2019.117232.
[6] J.P. Romualdi, J.A. Mandel, Tensile strength of concrete affected by uniformly distributed closely spaced short lengths of wire reinforcement, ACI J. 61 (1964) 657–671.
[7] N.P. Romualdi, G.B. Batson, Mechanics of crack arrest in concrete, ASCE Eng. Mech. 89 (1963) 147–168.
[8] F. Liu, W. Ding, Y. Qiao, Experimental investigation on the tensile behavior of hybrid steel-PVA fiber reinforced concrete containing fly ash and slag powder, Constr. Build. Mater. 241 (2020) 118000, https://doi.org/10.1016/j.conbuildmat.2020.118000.
[9] J.-P. Charron, C. Desmettre, C. Androuët, Flexural and shear behaviors of steel and synthetic fiber reinforced concretes under quasi-static and pseudo-dynamic loadings, Constr. Build. Mater. 238 (2020) 117659, https://doi.org/10.1016/j.conbuildmat.2019.117659.
[10] S. Rafid, A case study on concrete column strength improvement with different steel fibers and polypropylene fibers, J. Mater. Res. Technol. 8 (2019) 6106–6114.
[11] C.C. Thong, D.C.L. Teo, C.K. Ng, Application of polyvinyl alcohol (PVA) in cement-based composite materials: a review of its engineering properties and microstructure behavior, Constr. Build. Mater. 107 (2016) 172–180.
[12] T. Horikoshi, A. Ogawa, T. Saito, Properties of Polyvinyl Alcohol Fiber as Reinforcing Materials for Cementitious Composites, International Union of Laboratories and Experts in Construction Materials Systems and Structures, 2006, pp. 145–153.
[13] S. Hamoush, T. Lebdeh, T. Cummins, Deflection behavior of concrete beams reinforced with PVA micro-fibers, Constr. Build. Mater. 24 (2010) 2285–2293.
[14] D. Meng, T. Huang, Y.X. Zhang, C.K. Lee, Mechanical behaviour of a polyvinyl alcohol fibre reinforced engineered cementitious composite (PVA-ECC) using local ingredients, Constr. Build. Mater. 141 (2017) 259–270.
[15] A. Noushini, K. Vessalas, B. Samali, Static mechanical properties of polyvinyl alcohol fibre reinforced concrete (PVA-FRC), Mag. Concr. Res. 66 (9) (2014) 465–483.
[16] J.-X. Lin, Y. Song, Z.-H. Xie, Y.-C. Guo, B. Yuan, J.-J. Zeng, X. Wei, Static and dynamic mechanical behavior of engineered cementitious composites with PP and PVA fibers, J. Build. Eng. 29 (2020) 101097, https://doi.org/10.1016/j.jobe.2019.101097.
[17] S. Wang, Micromechanics Based Matrix Design for Engineered Cementitious Composites (PhD Thesis), University of Michigan, 2005.
[18] A.S. Shanour, M. Said, A.I. Arafa, A. Maher, Flexural performance of concrete beams containing engineered cementitious composites, Constr. Build. Mater. 180 (2018) 23–34.
[19] M. Said, A.A. Abd El-Azim, M.M. Ali, H. El-Ghazaly, I. Shaaban, Effect of elevated temperature on axially and eccentrically loaded columns containing Polyvinyl Alcohol (PVA) fibers, Eng. Struct. 204 (2020) 110065, https://doi.org/10.1016/j.engstruct.2019.110065.
[20] D. Meng, C.K. Lee, Y.X. Zhang, Flexural and shear behaviours of plain and reinforced polyvinyl alcohol-engineered cementitious composite beams, Eng. Struct. 151 (2017) 261–272.
[21] A. Alyousif, O. Anil, M. Sahmaran, M. Lachemi, G. Yildirim, A.F. Ashour, Comparison of shear behaviour of engineered cementitious composite and normal concrete beams with different shear span lengths, Mag. Concr. Res. 68 (5) (2016) 217–228.
[22] K.M.A. Hossain, S. Hasib, T. Manzur, Shear behavior of novel hybrid composite beams made of self-consolidating concrete and engineered cementitious composites, Eng. Struct. 202 (2020) 109856, https://doi.org/10.1016/j.engstruct.2019.109856.
[23] M.A. Adam, M. Said, A.A. Mahmoud, A.S. Shanour, Analytical and experimental flexural behavior of concrete beams reinforced with glass fiber reinforced polymers bars, Constr. Build. Mater. 84 (2015) 354–366.
[24] H.-L. Dong, W. Zhou, Z. Wang, Flexural performance of concrete beams reinforced with FRP bars grouted in corrugated sleeves, Compos. Struct. 215 (2019) 49–59.
[25] D. Pawłowski, M. Szumigała, Flexural behavior of full-scale basalt FRP RC beams experimental and numerical studies, Procedia Eng. 108 (2015) 518–525.
[26] D. Tomlinson, A. Fam, Performance of Concrete Beams Reinforced with Basalt FRP for Flexure and Shear, J. Compos. Constr. 19 (2) (2015) 04014036, https://doi.org/10.1061/(ASCE)CC.1943-5614.0000491.
[27] D. Douglas, An Investigation into the Flexural Behavior of GFRP Reinforced Concrete Beams [MSc thesis], University of Toronto, Canada, 2012.
[28] Z. Soric, T. Kisicek, J. Galic, Deflections of concrete beams reinforced with FRP bars, Mater Struct 43 (S1) (2010) 73–90.

[29] F. Raffaello, P. Andrea, A. Domenico, Limit States Design of Concrete Structures Reinforced with FRP Bars, [Ph.D. thesis], Italy, University of Naples Federico.
[30] Y. Tu, J. Zhang, Y. Qian, Experimental and theoretical investigation of flexural load-carrying capacity of concrete beams reinforced with AFRP tendons, J. Southeast Univ. (Nat. Sci.), China 39 (3) (2009) 563–568.
[31] M.N. Habeeb, A.F. Ashour, Flexural behavior of continuous GFRP reinforced concrete beams, J. Compos. Constr. 12 (2) (2008) 115–124.
[32] M. Pecce, G. Manfredi, E. Cosenza, Experimental response and code models of GFRP RC beams in bending, J. Compos. Constr. 4 (4) (2000) 182–190.
[33] M. Said, M.A. Adam, A.A. Mahmoud, A.S. Shanour, Experimental and analytical shear evaluation of concrete beams reinforced with glass fiber reinforced polymers bars, Constr. Build. Mater. 102 (2016) 574–591.
[34] W.-J. Ge, A.F. Ashour, J. Yu, P. Gao, D.-F. Cao, C. Cai, X. Ji, Flexural behavior of ECC–concrete hybrid composite beams reinforced with FRP and steel bars, J. Compos. Constr. 23 (1) (2019) 04018069, https://doi.org/10.1061/(ASCE)CC.1943-5614.0000910.
[35] W. Qu, X. Zhang, H. Huang, Flexural behavior of concrete beams reinforced with hybrid (GFRP and steel) bars, J. Compos. Constr. 13 (5) (2009) 350–359.
[36] Z. Sun, L. Fu, D.-C. Feng, A.R. Vatuloka, Y. Wei, G. Wu, Experimental study on the flexural behavior of concrete beams reinforced with bundled hybrid steel/FRP bars, Eng. Struct. 197 (2019) 109443, https://doi.org/10.1016/j.engstruct.2019.109443.
[37] A. El Refai, F. Abed, A. Al-Rahmani, Structural performance and serviceability of concrete beams reinforced with hybrid (GFRP and steel) bars, Constr. Build. Mater. 96 (2015) 518–529.
[38] W. Ge, J. Zhang, D. Cao, Y. Tu, Flexural behaviors of hybrid concrete beams reinforced with BFRP bars and steel bars, Constr. Build. Mater. 87 (2015) 28–37.
[39] I.F. Kara, A.F. Ashour, M.A. Köroğlu, Flexural behavior of hybrid FRP/steel reinforced concrete beams, Compos. Struct. 129 (2015) 111–121.
[40] M.A. Safan, Flexural behavior and design of steel–GFRP reinforced concrete beams, ACI Mater. J. 110 (6) (2013) 677–685.
[41] D. Lau, H.J. Pam, Experimental study of hybrid FRP reinforced concrete beams, Eng. Struct. 32 (12) (2010) 3857–3865.
[42] M.A. Aiello, L. Ombres, Structural performances of concrete beams with hybrid reinforcements, J. Compos. Constr. 6 (2) (2002) 133–140.
[43] H.Y. Leung, R.V. Balendran, Flexural behavior of concrete beams internally reinforced with GFRP rods and steel bars, Struc. Surv. 21 (2003) 146–157.
[44] G.u. Xingyu, D. Yiqing, J. Jiwang, Flexural behavior investigation of steel-GFRP hybrid-reinforced concrete beams based on experimental and numerical methods, Eng. Struct. 206 (2020) 110117, https://doi.org/10.1016/j.engstruct.2019.110117.
[45] X. Ruan, C. Lu, K.e. Xu, G. Xuan, M. Ni, Flexural behavior and serviceability of concrete beams hybrid-reinforced with GFRP bars and steel bars, Compos. Struct. 235 (2020) 111772, https://doi.org/10.1016/j.compstruct.2019.111772.
[46] M. Ju, S. Lee, C. Park, Response of glass fiber reinforced polymer (GFRP)-steel hybrid reinforcing bar in uniaxial tension, Int. J. Concr. Struct. Mater. 11 (4) (2017) 677–686.
[47] U. Priyanka, M.E. Siva, Hybrid reinforcement by using GFRP, Int. Res. J. Eng. Technol. 3 (2016) 642–645.
[48] K.T. Park, Y.K. Hyeong, J.Y. Young, Y.L. Sang, W.S. Dong, Hybrid FRP Reinforcing Bars for Concrete Structures, in: Fourth Asia-Pacific Conference on FRP in Structures, International Institute for FRP in Construction, Melbourne, Australia, 2013.
[49] E. Etman, Flexural Performance of RC Slabs with Internal Hybrid Reinforcement, in: 5th IECC'5, American Society of Civil Engineers, August 2008.
[50] ANSYS–Release Version 12.1.0, A Finite Element Computer Software and User Manual for Nonlinear Structural Analysis, ANSYS Inc. Canonsburg, PA, 2009.
[51] Datafit Version 9.1, Curve Fitting Non-linear Regression and Data Plotting Software, Oakdale Engineering, 2019.
[52] M.F. Nuruddin, S. Ullah Khan, N. Shafiq, T. Ayub, Strength prediction models for PVA fiber-reinforced high-strength concrete, J. Mater. Civ. Eng. 27 (12) (2015) 04015034, https://doi.org/10.1061/(ASCE)MT.1943-5533.0001279.
[53] E. Montoya, F. Vecchio, S.A. Sheikh, Compression field modelling of confined concrete, J. Struct. Eng. Mech. 12 (3) (2001).
[54] ACI Committee 318, Building code requirements for structural concrete, ACI 318-18, 2018.
[55] American Concrete Institute (ACI), Guide for the Design and Construction of Concrete Reinforced with FRP Bars, ACI 440.1R-03, ACI Committee 440, Farmington Hills, Michigan, 2003, p. 42.